（千葉大学審査学位論文）

AMSR-E soil moisture evaluation over Shanxi Province of China and spatio-temporal characteristics of soil moisture distribution in East Asia

August 2016

Chiba University

Graduate School of Science

Division of Geosystem and Biological Sciences

Department of Earth Sciences

Mei SUN

ABSTRACT

Soil moisture is a crucial hydrological parameter in studies of Earth's surface heat budget and climate changes. In recent decades, long-term estimation of soil moisture on global scales has become possible through satellite remote sensing. Among the existing satellite datasets, microwave observations provide the best estimates of soil moisture because the dielectric constants differ between soil and water. A successful microwave mission is the Advanced Microwave Scanning Radiometer for EOS (AMSR-E), a passive microwave detector that provides the global daily moisture levels of surface soils. These data are highly important in studies of land–atmosphere interactions. Although the AMSR-E product has been widely validated and applied in previous studies, its performance in East Asia, the region of the most intensive human activity in the world, has not been thoroughly evaluated.

Consequently, this study addresses two main research objectives. The first is to evaluate AMSR-E soil moisture from in situ datasets collected at 109 observation stations in Shanxi Province, China, and to analyze the relationships among soil moisture, elevation, complexity of topography (standard deviation of elevation), precipitation (hydrological factor), NDVI (vegetation factor), and land use types in this province. The second objective is to reveal the spatio-temporal characteristics of the soil moisture distribution in various areas of East Asia, based on the validation results of AMSR-E soil moisture.

To compare the in situ soil moisture with the AMSR-E data, we averaged the in situ soil moisture at high spatial resolution within a (50 × 50) km^2. Comparisons were performed from 28th April to 18th September in 2006 and 2007. The data from 64 of the 109 observation stations were reasonably consistent with the in situ measurements (correlation coefficient > 0.5). Thus, the AMSR-E soil moisture measurements were acceptably accurate over Shanxi Province of China. High correlation coefficients (>0.7) were found in areas with uniform land use types and relatively flat terrain. For the same land use types

and similar topographic complexity, the correlation coefficient was higher in areas containing more in situ observation stations in the (50 × 50) km^2 window area. The average AMSR-E soil moisture over the whole Shanxi Province were well correlated with the soil moisture averaged over 109 in situ observation stations (correlation coefficient = 0.93). The daily AMSR-E soil moisture distribution also well corresponded to the daily precipitation in areas of heterogeneous land use type and complex terrain. These results demonstrate the high performance of the AMSR-E soil moisture in areas densely installed with in situ observation stations.

The AMSR-E soil moisture tended to increase from northwest to southeast of Shanxi Province. This spatial tendency corresponded to the precipitation gradient on annual, monthly and daily time scales. However, discrepancies between soil moisture and precipitation were also found. These were attributed to the different observation times of the satellite overpass and the in situ observations of soil moisture, and to irrigation of the agricultural areas in the time series analysis. The AMSR-E soil moisture is also well correlated with SPOT/VEGETATION NDVI data. However, soil moisture is difficult to estimate in dense forest areas.

After confirming the performances of the AMSR-E soil moisture, the date set was further analyzed in two representative East Asian regions (the middle and lower Yangtze River plain and Sichuan Basin) from 2003 to 2009. The characteristics and variations of soil moisture distributions depend on various environmental conditions and local land use types. The distribution of the AMSR-E soil moisture followed the movement of the Baiu front and captured the 2003 flood records at Bengbu near Huaihe River. In Sichuan Basin, the precipitation was not directly related to soil moisture distribution, because the latter was modified by human activities (irrigation). As the rice farming calendar in Sichuan Basin includes two cropping seasons, two soil moisture peaks were observed during each year. The increasing and decreasing tendencies of AMSR-E soil moisture are consistent with the

rice transplanting and harvest seasons. In addition, after a rainfall event, humid regions retain high soil moisture for several days longer than arid and semi-arid regions. These trends were inferred in comparisons of three areas (humid, arid, and semi-arid) in China from 2002 to 2009.

ACKNOWLEDGEMENTS

I would like to express gratitude to my adviser, Dr. A. Kondoh, Professor of Center for Environmental Remote Sensing, Chiba University, for granting me the opportunity to visit Japan as a research student, and also for his continuing encouragements and guidance during the graduate work and research. Throughout the four years of my doctoral course, I learned remote sensing technology, geography and hydrology, and became especially experienced at microwave remote sensing and soil moisture variation by satellite.

I also thank Prof. Kaihotsu at Hiroshima University for giving me valuable suggestions and guidance to improve my research and paper, and Prof. Ai at the Chinese Academy of Sciences for providing the soil moisture monitoring data of Shanxi Province. Thanks are also extended to the members of Kondoh's laboratory, whose ideas helped me solve technical computing issues with the remote sensing data and spatial analysis.

Thank you to my family members, who supported my overseas education both mentally and financially all the time.

TABLE OF CONTENTS

LIST OF TABLES

LIST OF FIGURES

Chapter I. Introduction

1.1 Previous studies of soil moisture

Soil moisture (or soil moisture content) plays an important role in the hydrological cycle and climate change. Soil moisture can be defined in various ways. The usual definition is the water content in the unsaturated soil zone (Hillel, 1998). The amount of water in the spaces between the soil particles determines the actual soil moisture. In previous studies, soil moisture was variously classified as root-zone soil moisture, surface soil moisture and others. The root-zone water content in the upper two meters of soil has been measured by volumetric, gravimetric and several other methods (Klemas *et al.,* 2014). The root-zone soil moisture largely controls the exchange of water and energy budgets (Sabater *et al.,* 2007). Surface soil moisture can be detected by satellite remote sensing technologies operating at optical, thermal infrared, and microwave (active and passive) wavelength. All of these technologies can measure the soil moisture in the upper soil layer (0–5 cm) (Njoku *et al*., 2003). This thinner soil layer is considered as the most different points when measuring land surface soil moisture. In this study, we investigate only the surface soil moisture of land.

The importance of soil moisture has been widely reported. Figure 1.1 shows the global climate system in 2007 (IPCC, 2007). The system is dominated by a large circulation of water, which changes its phase from the atmosphere to underground. Examples of phase changes are water vapor, precipitation, soil moisture, and groundwater. The water route and volume also change throughout this system. Precipitation infiltrates and sinks into the soil water belt. Later, this water can return to the atmosphere through evaporation. Thus, soil moisture is a critical boundary between land surfaces and the atmosphere. Soil moisture is also monitored for irrigation scheduling of agriculture (Moran, 1994). In continental climate systems, soil moisture can predict the land surface conditions and improve weather

forecasts. As a hydrologic drought index, it provides early warning in areas vulnerable to droughts or floods. In global environmental studies, it can monitor yellow dust, soil degradation, global warming, and other important phenomena (Shinoda, 2005).

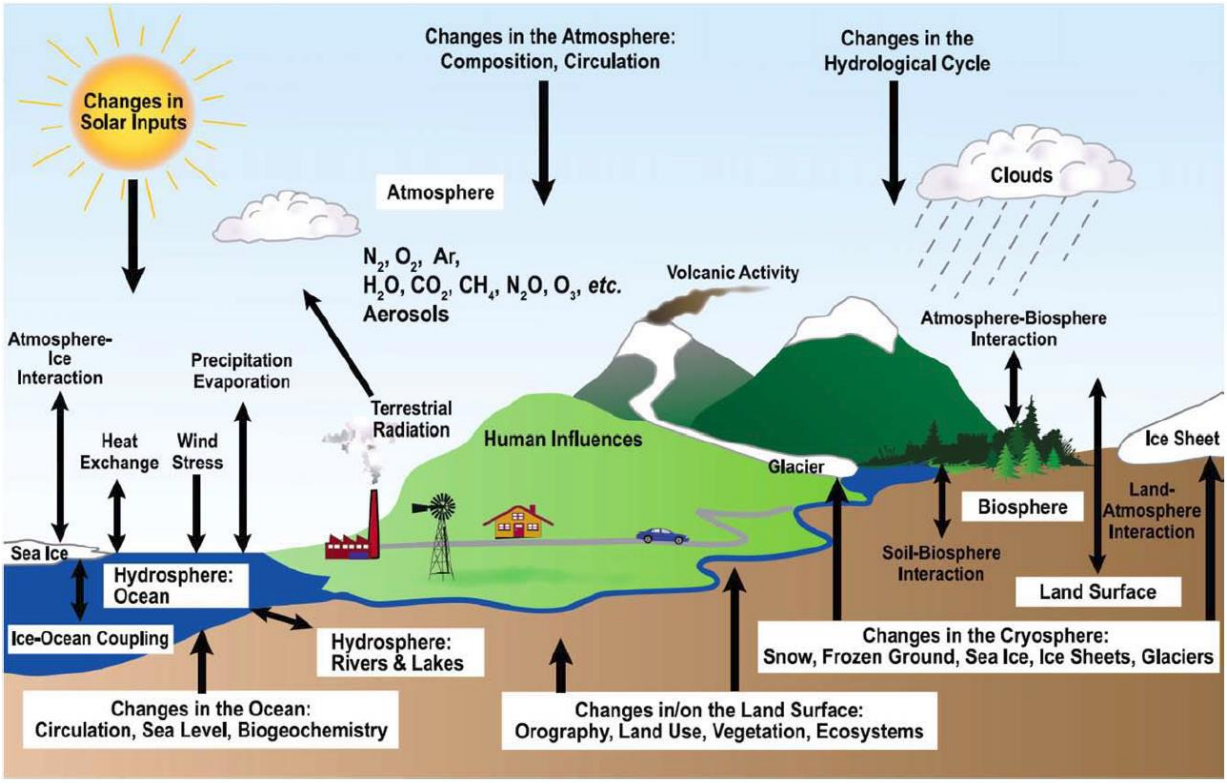

Figure 1. 1 Global climate system (IPCC, 2007).

Although soil moisture is very important, its information is not easily acquired over a large area. The first wide-area soil moisture monitoring system was created for harvest prediction by the former Soviet Union in the 1930s. Local gravimetric observations of soil moisture were obtained three times per month during the warm season and once per month during the winter, amounting to over 3000 observations after 20 years. Delworth *et al.* (1988) recognized and evaluated soil moisture in climate variability. However, the results of these land-surface process models disagreed with each other and with observed soil moisture. In July of 1993, flooding occurred near the Mississippi river in the Midwestern USA. This sustained flooding event was linked to high soil moisture, which was retained after the spring rains. In a first attempt at predicting flooding from surface wetness, the soil

moisture was input to a short-range atmospheric model. The accuracy of the flood forecast was noticeably improved (Beljaars *et al.,* 1996). Surface wetness in land models predicts precipitation events with strong reproducibility, and could re-simulate the Mississippi flood phenomenon. Soil moisture is generally thought to enhance flooding conditions (Seth and Giorgi 1998, Bosilovich and sun 1998, Pal and Eltahir 2001). Networks of agricultural stations provide distributed point measurements, but are insufficient for estimating soil moisture over large areas with spatial and temporal variability (Njoku *et al*., 2003). Recently, soil moisture observation networks for long-term monitoring have been established in Australia (Rudiger *et al.,* 2007), and by the Meteorological Automatic Network Integrated Application (MANIA) in south-western France (Calvet *et al.*, 2007). However, these installations were costly to install and were still restricted to single-point observations. Currently, satellite monitoring is considered as the only feasible technique for global, long-term observations of soil moisture, because they detect the dielectric properties of soil and water (Chaurasia *et al.*, 2011, Wang *et al*., 2009)

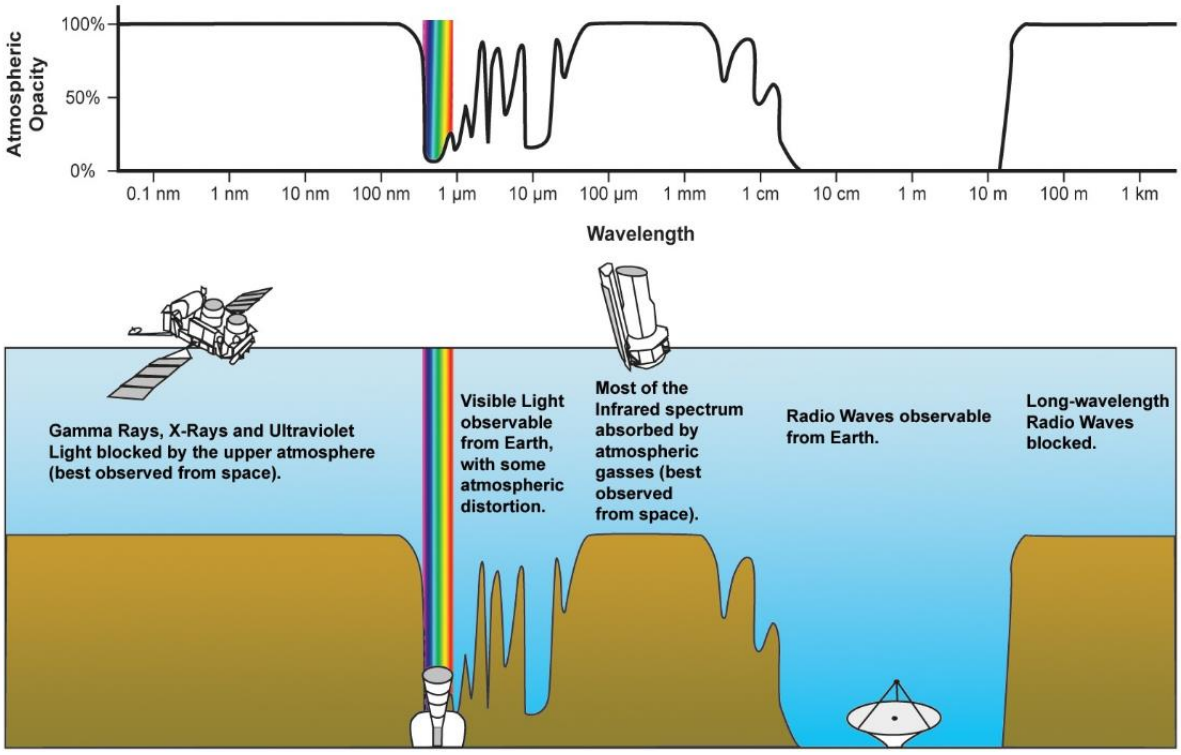

Figure 1. 2 Atmospheric electromagnetic opacity (NASA, 2008).

In recent years, soil moisture information has been acquired from many sensors orbiting in space. These sensors differ primarily by their wavelength spectra. Figure 1.2 shows the electromagnetic opacity in the Earth's atmosphere (NASA, 2008). Most of the infrared spectrum is absorbed by atmospheric gasses. The microwave portion of the electromagnetic spectrum ranges from approximately one millimeter to one meter. Because of their longer wavelengths (lower frequencies) than visible and infrared waves, microwaves possess special properties that are critical for remote sensing. For instance, microwave frequencies (50 GHz; $\lambda = 0.6$ cm) are easily transmitted through dry air. A large water vapor content increases the absorption and reduces the transmittance. Microwave radiation can penetrate cloud cover, haze and dust, and is unaffected by atmospheric scattering. As microwave sensors receive the electromagnetic energy naturally emitted by an observed object, the radiometric temperature of objects at the earth's surface is called the brightness temperature. Conversely, the soil dielectric constant depends on the soil moisture and is related to emissivity. The emissivity and brightness temperature are negatively correlated. Brightness temperature measurements are the essence of microwave remote sensing.

In this study, land-surface soil moisture is determined by passive microwave remote sensing. Some passive microwave sensors that measure soil moisture are outlined below. The Scanning Multichannel Microwave Radiometer (SMMR) on the Nimbus-7 satellite of the National Aeronautics and Space Administration (NASA) operated for over eight years, from 26th October 1978 to 20th August 1987. This ten-channel instrument provides polarized antenna temperature data at five microwave wavelengths. The Special Sensor Microwave/Imager (SSM/I), which has operated on the Defense Meteorological Satellite Program (DMSP) satellite since 1987, is a near-polar orbiting satellite. The Tropical Rainfall Measuring Mission's Microwave Imager (TRMM) was launched on 27th November, 1997. This imager carries five instruments, one of which is a multi-channel,

dual-polarized passive microwave radiometer called the TRMM Microwave Imager (TMI). To better understand the Earth's water cycle, the European Space Agency (ESA) mission, the NASA hydrosphere states mission and the Soil moisture Active and Passive mission (SMAP) launched the Soil Moisture and Ocean Salinity (SMOS) satellite on 2nd November, 2009. The Advanced Microwave Scanning Radiometer-Earth Observing System (AMSR-E) on the Aqua satellite operated from 4th May, 2002 to 4th October, 2011 (over 9 years). It was designed and developed by the Japan Aerospace Exploration Agency (JAXA) in collaboration with the U.S. AMSR-E, a modification of AMSR installed on the ADEOS-II satellite, observes global-scale water bodies such as ocean ice, surface temperatures and soil water. However, the soil moisture obtained by AMSR-E contain uncertainties sourced from the instrument calibration, inversion algorithm, geophysical noise and others sources (Eymard *et al.,* 1993). Therefore, the accuracy of remote sensing data must be evaluated before use. In this paper, we validate and estimate the soil moisture collected by the AMSR-E sensor only.

Table 1.2 summarizes the properties of the AMSR-E instrument. With a swath width of approximately 1450 kilometers, AMSR-E observes the whole planet in approximately 2 days. The Aqua orbit is sun-synchronous with the equator and crosses Japan at 1:30 PM and 1.30 AM local time. Worldwide, soil moisture data are analyzed by four main algorithms in the world; Njoku *et al.* (2003) by NASA, Koike *et al.* (2004) by JAXA, Jackson (1993) by the United States Department of Agriculture, and Owe *et al.* (2001) by a collaboration between the University of Amsterdam and JAXA. The accuracies of the soil moisture estimated by these algorithms was discussed at the evaluation meeting of the JAXA-NASA AMSR/AMSR-E Joint Committee (Koike *et al.,* 2009). The latest AMSR-E soil moisture algorithm developed in Japan was reported as the most accurate among these main algorithms.

Table 1. 1 Characteristics of the AMSR-E instrument (Njoku *et al*., 2003).

Center Frequency (GHz)	6.925	10.65	18.7	23.8	36.5	89.0 A	89.0 B
Band Width (MHz)	350	100	200	400	1000	3000	
Polarization	Vertical and Horizontal						
Sampling Interval (km)	9 × 10					4.5 × 4	4.5 × 6
Temperature Sensitivity (K)	0.34	0.7	0.7	0.6	0.7	1.2	1.2
Incidence Angle (°)	55.0						54.5
Dynamic Range (K)	2.7–340						
Swath Width (km)	Approximately 1450						
Integration Time (ms)	2.5					1.2	
Quantization (bit)	12	10					
Scan Cycle (s)	1.5						

The Koike soil moisture algorithm proceeds in three main steps. Step One optimizes the parameters of the forward model using the radiative transfer equation. Because the AMSR-E can measure the brightness temperature, we can generate a fully physical radiative transfer model. The model is formulated as

$$T_b = exp(-\Gamma_c) \cdot Es \cdot Ts + (1-\omega_c)[1-exp(-\Gamma_c)]T_c \quad , \qquad (1.1)$$

where T_b is the brightness temperature measured by the AMSR-E radiometer, Γ_c is the optical depth of the canopy, and *Es* is the soil emissivity, which depends on the soil moisture type. ω_c is the single scattering albedo of the canopy, which is here set to zero. *Ts*

and T_c represent the physical temperatures of the soil and canopy, respectively. The first term in the right-hand side of Eq. (1.1) describes the surface emission; the second describes the upward radiation from the vegetation layer. The four variables in this equation are the soil moisture content, plant water content, vegetation temperature, and soil temperature.

Step Two is the index generator of the algorithm. Koike *et al*., (2004) proposed two indexes, the soil moisture (*ISW*) and polarization index (*PI*), to obtain the soil moisture content and the soil moisture content under the assumption of equal vegetation and soil temperatures. Originally, the two indexes were defined as follows:

$$ISW = (T_{bi} - T_{bj}) / [(T_{bi} + T_{bj})/2], \quad (1.2)$$

$$PI = (T_{bv} - T_{bh}) / [(T_{bv} + T_{bh})/2], \quad (1.3)$$

where T_b is the brightness temperature of microwaves, *i* and *j* indicate high (36 GHz) and low (6 GHz) frequency respectively, and *v* and *h* represent vertical and horizontal polarization, respectively. For smooth surfaces, T_{bv} generally exceeds T_{bh}. The frequencies 36 and 6 GHz are carefully chosen. As the emissivity of water is small at low frequencies, a wider range improves the index calculation; on the other hand, receiver data are lost at 89 GHz, yielding incorrect brightness temperatures.

Step Three of the algorithm develops a look-up table inversion and soil moisture estimation. The look-up table confirms the relationship between *ISW* and *PI* (Figure 1.3*)*. The soil moisture is estimated by linear interpolation of the brightness temperature or indices in the inverted look-up table. According to the transform equation, the soil moisture ranges from 0% to 60% and the vegetation water content varies from 0 to 2. The brightness temperature is then derived by the forward model. The soil moisture is estimated from the lookup table. This algorithm is detailed in Lu *et al.*, (2009).

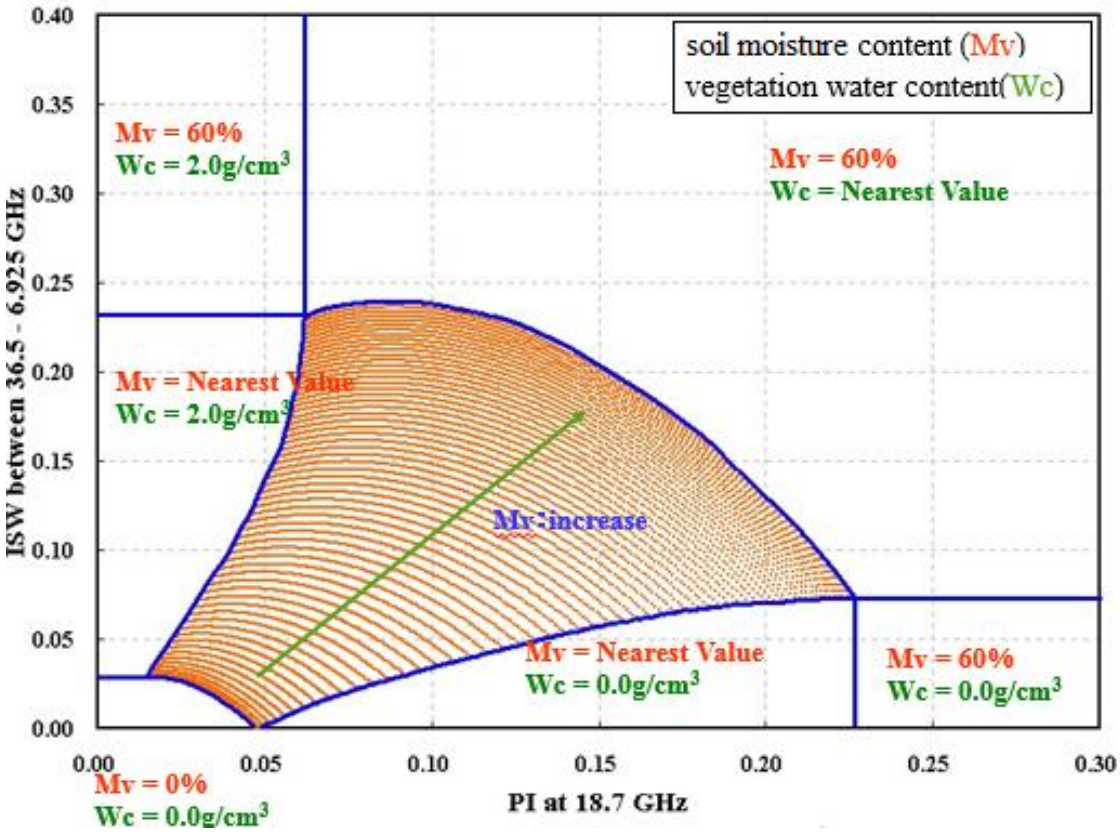

Figure 1. 3 Lookup table of soil moisture, ISW, and PI (provided by Kaihotsu).

AMSR-E soil moisture has been extensively researched in various geographical environments throughout the world. Assessment of the AMSR-E soil moisture in India identified a need to revisit the retrieval algorithm in different terrain regions (Chaurasia *et al.*, 2011). The soil moisture over Australia has been derived from ground-based soil moisture collected by AMSR-E (Draper *et al.*, 2009). The data were strongly correlated with those of the Murrumbidgee and Gouburn monitoring networks; moreover, the soil moisture corresponded to the long-term and short-term precipitation data across Australia. The AMSR-E soil moisture derived from the Land Parameter Retrieval Model (LPRM) algorithm was evaluated over South America (Rossato *et al.*, 2013). The correlation coefficients between the AMSR-E and in situ soil moisture was generally high (0.8 in most regions). These reliable soil moisture estimates might provide important information of events such as floods. Wangner *et al.* (2007) derived the near-surface soil moisture from AMSR-E over regions of Europe, and reported promising results. The AMSR-E soil

moisture product (Ver.5.0 of JAXA) has been estimated in the Mongolian Plateau (Kaihotsu *et al.,* 2009). Although the AMSR-E data were overestimated at some stations, they generally well-matched the ground-based monitoring data over a (120 × 160) km^2 study area.

However, because of manpower and material resources consumption, in situ soil moisture is limited in scope, they require validation by AMSR-E in many areas. Comparisons between satellite and in situ data of soil moisture at each observation station are insufficient. To evaluate satellite products without spatial variability errors, sampling stations need to be placed at one-pixel intervals (Kaihotsu et al., 2009). Few studies have investigated the effects of topography on soil moisture (Wigneron *et al.*, 2003), or the influences of land use patterns on soil moisture (Fu *et al.,* 2003). Chapter 3 of this thesis attempts to validate and estimate the soil moisture in Shanxi Province of China using an AMSR-E product-retrieval algorithm developed by JAXA. The correlations between the AMSR-E data and the spatio-temporal variations of soil moisture are discussed in terms of precipitation (hydrological factors), complexity of topography, land use and vegetation index (NDVI).

AMSR-E data are applicable not only to soil moisture, but to water-related phenomena around the planet, thus improving our understanding of climate changes. For instance, AMSR-E can measure the global distribution of the monthly averaged sea surface temperature and wind speed (Konda *et al.*, 2009). Through images of the AMSR-E sea surface temperature, fishing industries can designate special areas to increase their operational efficiency and reduce cost. AMSR-E data also provide the daily rainfall intensity. By investigating the relationship between rainfall intensity and short-wavelength data of AMSR-E, researchers have improved the method for estimating precipitation retrieval. AMSR-E can analyze the seasonal variation of sea ice concentration in the Arctic and Antarctic regions. Through sea ice observation using microwave radiometers, we can

detect signals of climate change. The Antarctic snow and ice distribution can be captured in a composite AMSR-E image. Multiple-frequency observations with AMSR-E can obtain the thermal fluctuations between the surface and deep snow layer on the ice sheet, and hence the short-term and long-term temperature changes. Atmospheric dynamics and thermodynamics can calculate the temporal changes in atmospheric variables from numerical weather predictions. In this way, the future state of the atmosphere can be predicted. In numerical weather prediction, heavy-rain forecasts improve when the AMSR-E perceptible water data are assimilated immediately before the expected downpour. The AMSR-E observation data provide more accurate predictions. Combined with sea wind data, AMSR-E also provides information on typhoons, enabling the monitoring and forecasting of typhoon generation. Such information is indispensable in operational weather observations. Furthermore, the soil moisture information provided by AMSR-E is relevant to agriculture (Michiura, 2011), and has been applied in monthly predictions of wheat, corn, and bean yields. However, paddy fields and growth predictions of food crops have not been investigated by these means. In addition, AMSR-E soil moisture has been rarely applied to movement of the rainy season. In Chapter Four of this thesis, AMSR-E soil moisture will be newly applied to both agriculture and the rainy season.

1.2 Objectives of this study

This thesis serve two main purposes. First, it evaluates the AMSR-E soil moisture product in comparisons with in situ data collected in Shanxi Province of China. For this purpose, it analyzes the relationships among soil moisture, precipitation, elevation, complexity of topography (quantified by the standard deviation of the elevation), vegetation index and land use. These analyses are represented in Chapter 3. The second objective is to analyze the spatial and temporal characteristics of the soil moisture distribution in different regions of East Asia. This objective also uses the AMSR-E soil moisture. Specifically, the growth conditions of paddy in Sichuan Basin are estimated by analyzing the daily changes in the

AMSR-E soil moisture. In a similar analysis, the soil moisture variation is related to natural factors (rainy season and flood records) and human activities. Both analyses are presented in Chapter 4.

1.3 Description of the study area

The research focuses on East Asia. As this is a large region, several regions are selected. The AMSR-E soil moisture is validated by in situ measurements of soil moisture collected in the Shanxi Province of China. Furthermore, the soil moisture changes described in Chapter 4 are analyzed in the middle and lower Yangtze River Plain and Sichuan Basin.

East Asia lies to the east of Eurasia, and includes Mongolia, China, North Korea, South Korea and Japan. The area covers approximately 11.7 million square kilometers. In this study, the AMSR-E soil moisture data set extends from 20°N to 55°N and 72°E to 136°E. As well as East Asia, this scope encompasses the south of Russia, part of India, and Bangladesh. Over such large-scale latitudes and longitudes, the natural environmental features will widely vary. Topographically, the area is lower in the east than in the west (Figure 1.4). The elevation ranges from −152 m to 8752 m under complicated geological conditions. At mid-latitudes, the huge coastal region is strongly affected by monsoon. In the western continental areas with less rainfall, there are the Gobi and Taklamakan deserts, the Himalayan Ranges, and the Tibet, and Mongolian Plateaus. From east to west of the continental region (covering ocean-sized distances), the climate changes are very obvious. The east coastal region of China is separated by two long rivers; the Yangtze River with a subtropical southern climate, and the Yellow River with a temperate northern climate. In addition, there are many mountains in North Korea, South Korea, and Japan. The total yield of paddy production exceeds 40% of the global production. Therefore, before analyzing the variation of soil moisture, we must understand the special regional characteristics of the area.

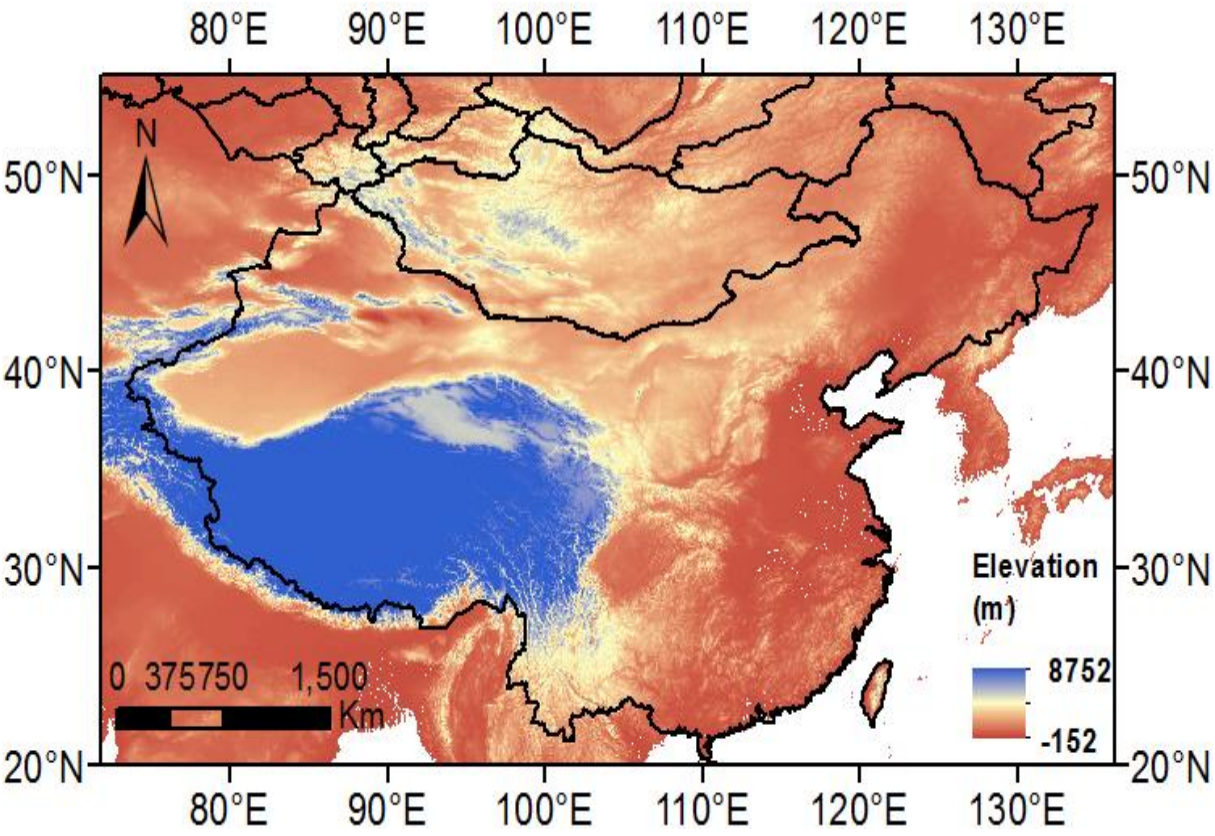

Figure 1.4 Elevation map of the study area.

Given that an in situ dataset of soil moisture (detailed in the next chapter) is available for Shanxi Province, we must clarify the terrain characteristics of this area. Shanxi Province is covered with yellow loess, which locates between longitudes 110.14°E and 114.33°E and latitudes 34.34°N to 40.43°N in north China. Figure 1.5 shows the 108 in situ soil moisture observation stations (black points) and the elevation of the study area, which is north-bounded by the Great Wall and Inner Mongolia. The south and west are bounded by Yellow River, Henan Province and Shaanxi Province. To the east lie the Taihang Mountains and Hebei Province. The east-to-west and north-to-south distances are approximately 370 km and 670 km, respectively, and the whole area is 156,266 km^2. A small percentage (1.64%) of this area is occupied by 11 small cities. The elevation ranges from 171 m to 3072 m, with 80% of the region occupied by mountains and hilly areas. Some basins are also present. The climate is temperate continental, with an annual mean temperature of 6.4°C and ranging from −11.3° in January to 21.8° in July. The annual mean

rainfall is between 400 mm and 650 mm (Niu *et al*., 2008). The in situ observation stations (black dots in Figure. 1.5) are concentrated on Taiyuan Basin in the central region, Linfen, Yuncheng Basin in the south and Changzhi Basin in the east.

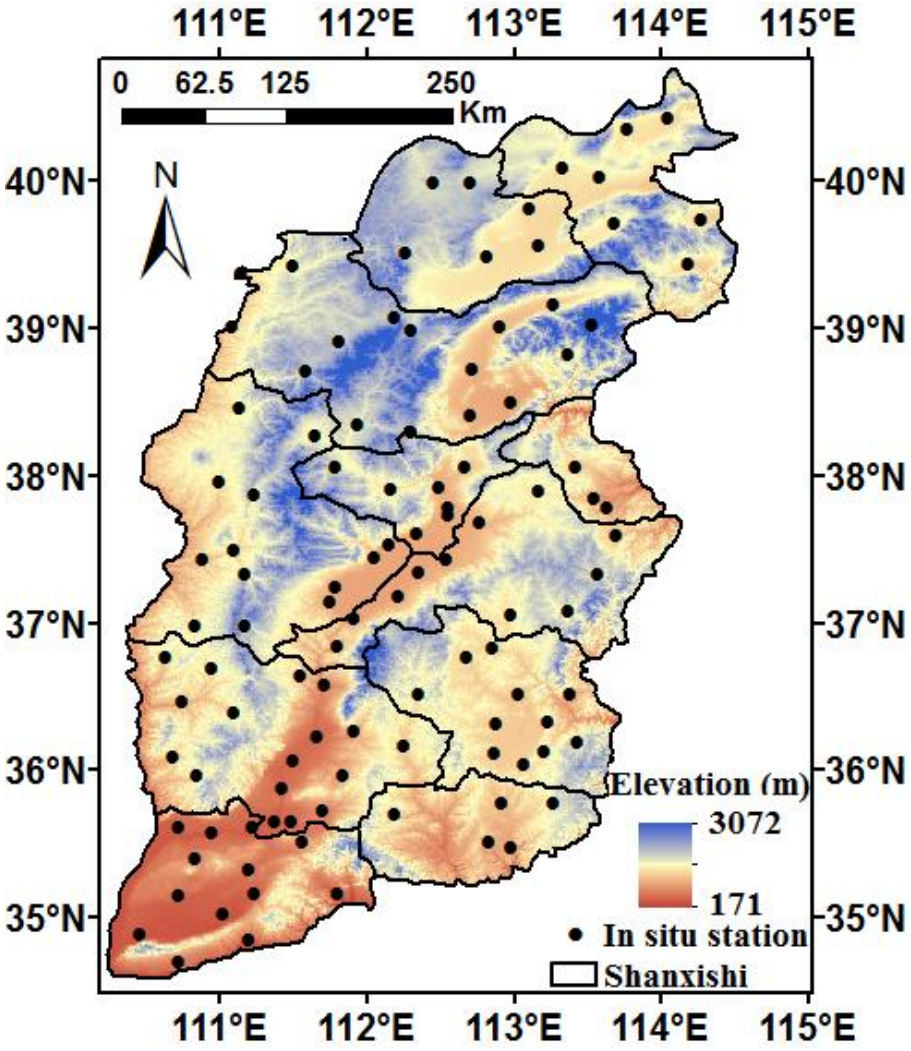

Figure 1. 5 Elevation and in situ soil moisture stations of Shanxi Province.

Chapter Ⅱ. Data and Methods

2.1 Data

Six datasets were analyzed in this study: 1) AMSR-E soil moisture dataset retrieved from the brightness temperatures, 2) in situ soil moisture obtained by the oven drying method, 3) a precipitation dataset freely downloaded from APHRODITE's Water Resources, 4) Normalized Difference Vegetation Indexes (NDVIs) from Spot/Vegetation satellite data, 5) Chinese 1 km mesh land use from China National Resources and Environment, and 6) ASTER GDEM (Digital Elevation Model) freely downloaded from NASA/ASTER satellite data. The second and third datasets are used to validate the AMSR-E soil moisture; the other datasets are used in regional-scale evaluations of the spatial and temporal variability of the soil moisture.

2.1.1 AMSR-E soil moisture data set

AMSR-E is a passive microwave radiometer (sensor) operated by JAXA. It was launched on the AQUA satellite of NASA in May of 2002, and its antenna stopped spinning in October of 2011. AMSR-E offers two main advantages; first, it measures weak, multi-frequency, dual-polarized microwaves from the Earth's surface and atmosphere; second, microwaves can detect soil moisture under all conditions (day and night, sunshine and rain).

The AMSR-E algorithm (Version 5.31) calculates the *ISW* and *PI* from the brightness temperatures, then obtains the soil moisture dataset from a look-up table (Koike *et al.*, 2002). The unit is volume of water content (m^3/m^3). The resolution (footprint) is 50 km by 50 km with resampling at 0.1° (10 km) intervals. In this study, we examine the descending pass of the daily AMSR-E soil moisture collected from July 2002 to May 2010.

2.1.2 In situ soil moisture data set

Within the study area, 109 in situ soil moisture locations are distributed across Shanxi Province They were installed by the Institute of Atmospheric Physics, Chinese Academy of Science. Each observation station records the longitude, latitude, elevation, and moisture content of the near-surface soil (depth 0–10 cm) by the oven drying method. The unit is the volumetric water content (m^3/m^3). The observing period excludes the winter months. They are April 8^{th}, 18^{th}, 28^{th}, May 8^{th}, 18^{th}, 28^{th}, June 8^{th}, 18^{th}, 28^{th}, July 8^{th}, 18^{th}, 28^{th}, Aug 8^{th}, 18^{th}, 28^{th}, September 8^{th}, 18^{th}, 28^{th} in both 2006 and 2007.

2.1.3 Precipitation data set

The daily precipitation dataset was obtained from APHRODITE's Water Resources (Asia Precipitation-Highly Resolved Observational Data Integration towards Evaluation of the Water Resources) project, which provides high-resolution grid data by setting rain gauges throughout the Asian region. The data were created by spatially interpolating between the satellite precipitation data and the in situ data, and were released in 2009 (Yatagai *et al*., 2009 ; Yatagai *et al*., 2012). In this study, we used the daily precipitation product (Version.V1003R1) of Monsoon Asia in 2006 and 2007, which is resolved to 0.25°.

2.1.4 Vegetation data set (SPOT Vegetation NDVI)

The vegetation index is a simple parameter based on the characteristics of light reflection. The commonest and most representative vegetation index is the NDVI, which evaluates the growth situation of vegetation. Here, the NDVI was derived from SPOT/VEGETATION and calculated as NDVI = (near-infrared band − visible band) / (near-infrared band + visible band). The NDVI value is expressed on a scale ranging from −1 to +1. In this study,

we used the Southeast Asia D 10 (10-day period synthesis) data, which is freely downloadable from the VITO website (Flemish Institute for Technological Research). These products provide a standard geometric sampling with a raw data resolution of approximately 1 km.

2.1.5 Land use dataset (Chinese 1 kilometer mesh land use)

The Chinese 1 kilometer mesh land use data were obtained from a project undertaken by China National Resources Environment Remote Sensing, which combines macro research and a dynamic information service system. The dataset contains 25 space layers (on the basis of Chinese National Standard GB/T21010-2007), each layer dedicated to the spatial distribution of a specific land use type. The spatial data are modeled as a 1 km mesh dataset. Any mesh area of 1 km^2 in each space layer is recognized as a percentage (%) of land use area. As an example, Figure. 2.1 displays the arable field ratio in the 2000s. Black areas contain no arable land. In the arable land areas, the ratio of arable field occupancy is indicated by the intensity of the blue color (the more intense the color, the higher the ratio). This dataset includes two periods; 1980s and 2000s. In this study we classified the main categories in the 2000s land use dataset, for correspondence with the in situ observation periods.

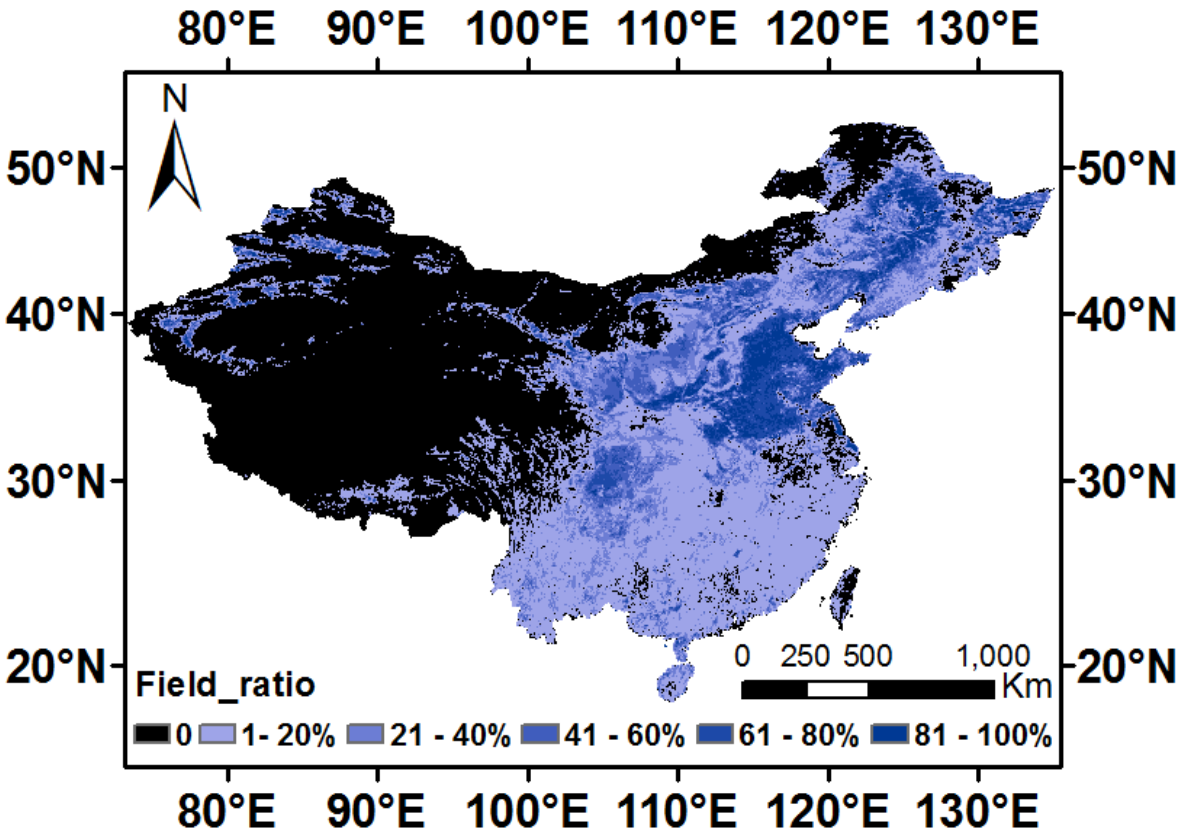

Figure 2. 1 Arable field distribution from Chinese 1 km mesh land use in the 2000s.

2.1.6 Elevation data set (ASTER Global DEM)

The Advanced Spaceborne Thermal Emission and Reflection Radiometer (ASTER) Global Digital Elevation Model (GDEM) was publicly released in 2009. The product was developed by NASA and Japan's Ministry of Economy, Trade, and Industry (METI). ASTER is a high-resolution 30-m imaging instrument installed on the Terra satellite. Its coverage is almost completely global (83°N–83°S). The whole area is covered with 226,000 tiles, each of (1° latitude × 1° longitude) containing at least 0.01% of the land area. To capture the terrain complexity, we obtained not only the elevation information of the study area but also the standard deviation of the elevaton in a (1 × 1) km^2 window.

2.2 Methods

2.2.1 Comparison of AMSR-E and in situ soil moisture

The AMSR-E soil moisture was validated against data from 108 observation locations (one location in Wutai Mountain is missing). As the resampling interval is 10 km, the footprint of the AMSR-E sensor is 50 km^2. A window size of five grids × five grids (50 km × 50 km) was selected. The average in situ soil moisture in the study area was calculated as

$$\text{In situ SM} = \frac{\sum(SM_1+SM_2+\ldots\ldots SM_N)}{N} \quad (2.1)$$

where SM is the soil moisture (m^3/m^3), and N is the number of observation stations.

The satellite soil moisture was then extracted and analyzed by their correlations between on the two datasets on the 8th, 18th and 28th from April to September in 2006 and 2007.

2.2.2 Spatial and temporal variation of AMSR-E soil moisture

Because frozen soil or snow obscures the real values of soil moisture (Koike *et al.*, 2004), this research investigates only the no-snow period (April to September) over Shanxi Province. Moreover, as the data are collected on a daily basis and the scanning width of the orbit is constrained, datasets are missing from some areas. Therefore, it is important to capture the short-time variation in soil moisture. This change is large after a rainfall, especially in arid and semi-arid areas (Shinoda, 2005). To determine the spatio-temporal moisture changes over Shanxi Province, we average the AMSR-E soil moisture over the first ten days of July, August and September in 2006 and 2007, and also the monthly maxima from April to September over the 2003–2009 period.

2.2.3 Relationship between AMSR-E soil moisture and NDVI

The surface soil moisture is also affected by the vegetation distribution (Njoku *et al*., 2003), which is commonly evaluated by the NDVI. In this research, the NDVI is evaluated for several reasons. First, very few soil moisture data were acquired over large areas during the 1980s and 1990s. Second, the NDVI can replace the soil moisture evaluation. Third, both NDVI and soil moisture content increase with increasing vegetation. Therefore, we here discuss the relationship between NDVI and soil moisture. To this end, the NDVI distribution map over Shanxi Province, created on July, August, and September of 2006 and 2007, was compared with the soil moisture variation over the same time scale (the first ten days of July, August, and September in 2006 and 2007). Because the resolutions differ between the two datasets, we converted the average NDVI pixel values to areas in five representative areas (for details, see Chapter 3):

$$NDVI = \frac{\sum(NDVI_{pixel1}+NDVI_{pixel2}+\ldots\ldots NDVI_{pixelN})}{N_{pixel}} \qquad (2.2)$$

where NDVI is the normalized difference vegetation index, and N is the number of pixels. The NDVIs can now be properly compared with the AMSR-E soil moisture.

Chapter III. Evaluation over Shanxi Province of China

3.1 Comparisons between AMSR-E and in situ soil moisture

To avoid snow cover artefacts in the analysis, we analyzed the ground-based observations from 28th April to 18th September in 2006 and 2007. Figure 3.1 shows the correlation coefficients (R) between the AMSR-E soil moisture and in situ soil moisture in both years (excluding the winter period) over Shanxi Province. The size of the black dots indicates the strength of the correlation. Throughout the region, the correlation coefficients range from 0.05 to 0.96. Higher values (>0.7) are concentrated in Taiyuan Basin (37°27'–38°25'N, 111°30'–113°09'E), Linfen Basin (36°04'–36°45'N, 111°3'–113°49'E), Yuncheng Basin (34°40'–35°38'N, 110°15'–110°46'E), Changzhi Basin (35°50'–37°08'N, 113°01'–113°40'E), and Yangquan Basin (37°27'–37°93'N, 113°10'–113°58'E). In Xinzhou, west Lvliang and the Linfen area, the correlation coefficients range are within the medium range (0.3–0.7). In these areas, the correlations are degraded by several anomalies. First, the ground-based datasets are point values with different spatial resolutions from the satellite data. Second, the correlations are biased by the different timings between the ground-based datasets and AMSR-E soil moisture monitoring. Third, the field data collection is influenced by various regional-scale natural and human factors. Therefore, the ideal correlation coefficients are difficult to achieve. The correlation coefficients in the northern parts (Datong and Shuozhou) were low (<0.3) in both years. Moreover, the validation results are limited to pixels, or (50 km × 50 km) areas, which contain different numbers of situ observation stations. Therefore, we also summarize the total in situ observation stations in each pixel. Figure 3.2 relates the correlation coefficients to the number of in situ observation stations in one grid during 2006 and 2007. The number of in situ observation stations per grid ranges from one to seven. The correlation coefficients improve with increasing density of in situ observation stations. Moreover, for the same number of

stations, the correlation coefficients could take high or low values, depending on site. For example, at one site with two in situ observation stations, the correlation coefficient was 0.1 (indicating no correlation); at another site with two observation stations, the correlation coefficient exceeded 0.8 (indicating very good correlation). These variations may result from complex topography, variable land use, and other factors.

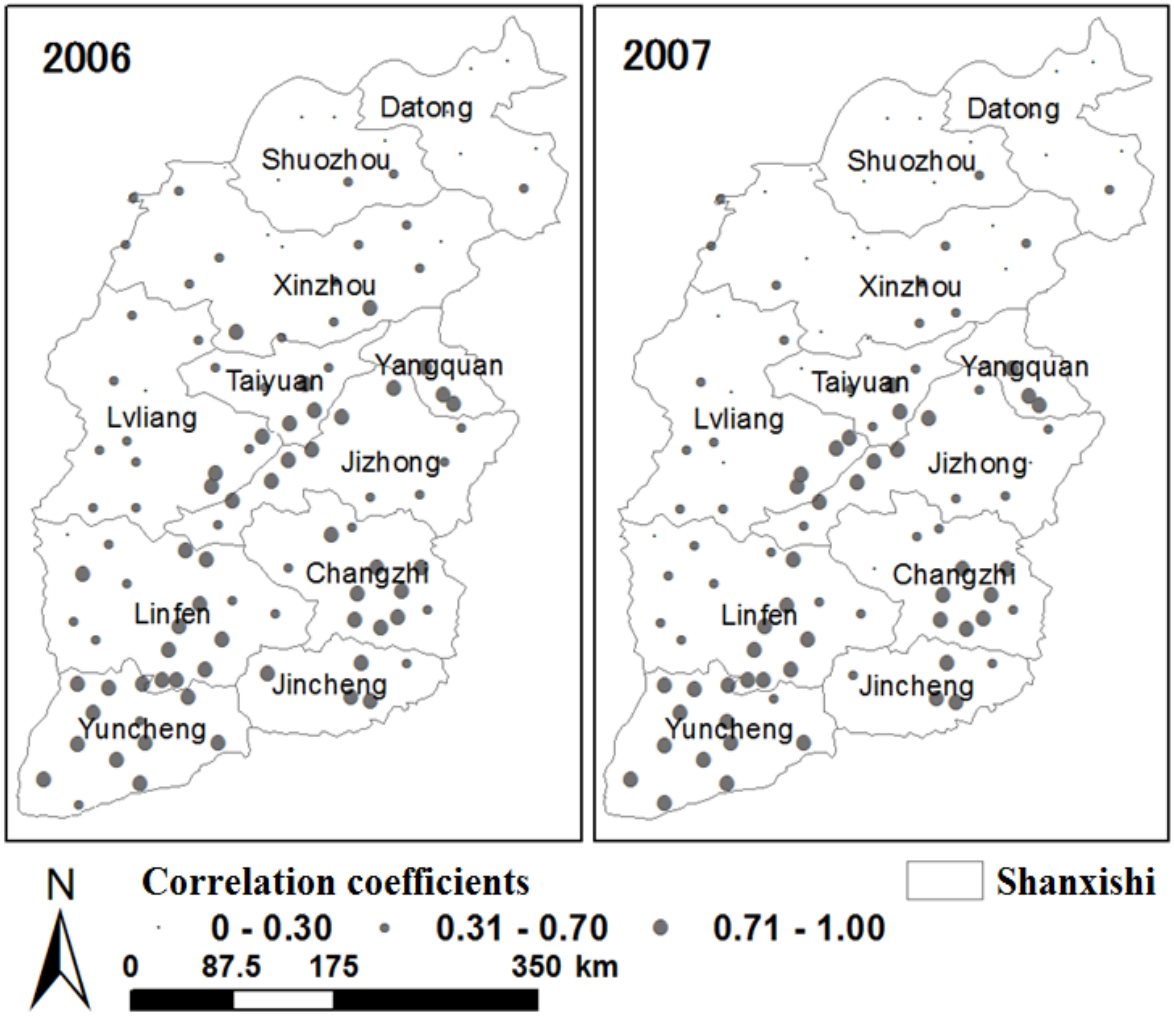

Figure 3. 1 Correlation coefficients between AMSR-E soil moisture and in situ soil moisture in 2006 and 2007 (28th April to 18th September).

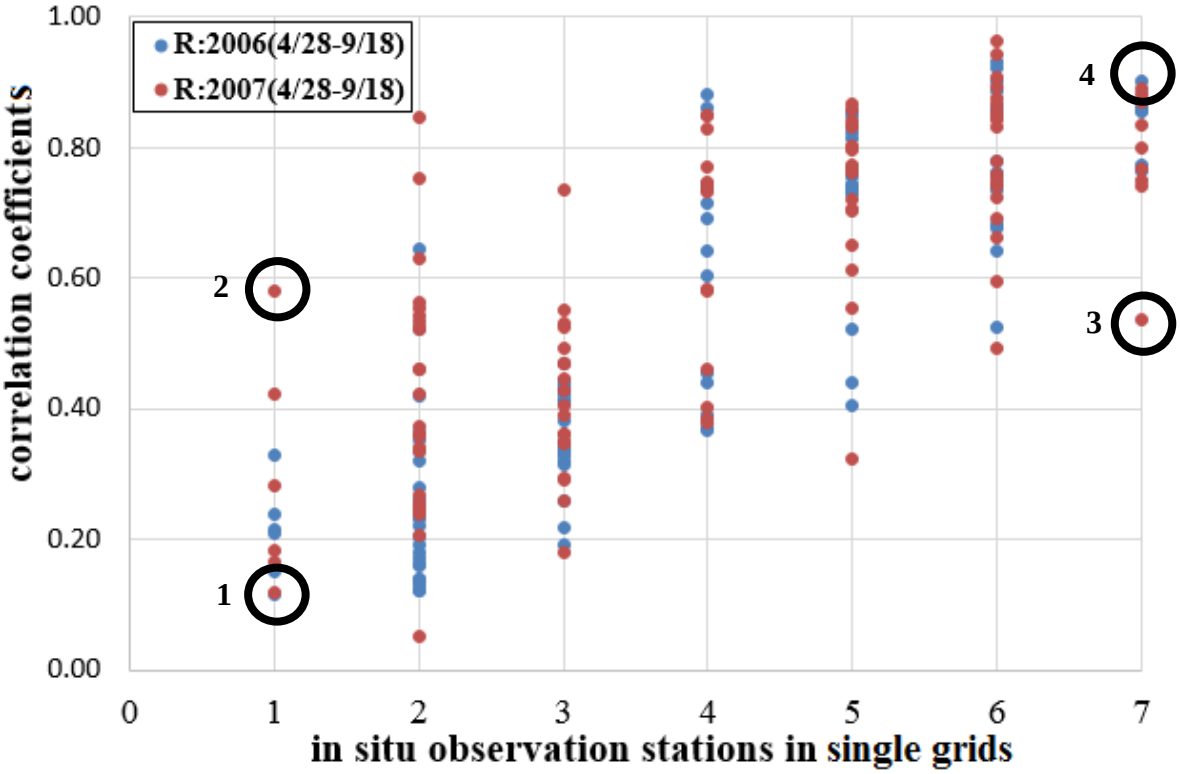

Figure 3. 2 Relationship between correlation coefficients and in situ observations stations in single grids.

3.1.1 Complexity of topography

To elucidate why the correlation coefficients differ at sites with the same number of in situ observation stations, we analyze the complexity of the topography in this section, and the land use in the succeeding section. Figure 3.3 presents the standard deviation of the 30-m resolution DEM in the (1 × 1) km^2 window, which represents the complexity of the terrain. The standard deviation is small in the basin areas and large throughout the mountainous areas to the east of Datong, Shuozhou and Xinzhou. In general, high correlation coefficients are associated with small standard deviations (relatively flat terrain). Figure 3.4 relates the correlation coefficient to the elevation and its standard deviation at the 108 in situ stations. Larger blue dots indicate higher correlation coefficients. Higher correlation coefficients (>0.7) are concentrated in two areas; one elevated at 400–600 m, the other at 800–1000 m. In both areas, the standard deviation of the elevation is approximately 10 m. The two areas are located in the south (Linfen Basin

and Yuncheng Basin) and the central region (Taiyuan Basin).

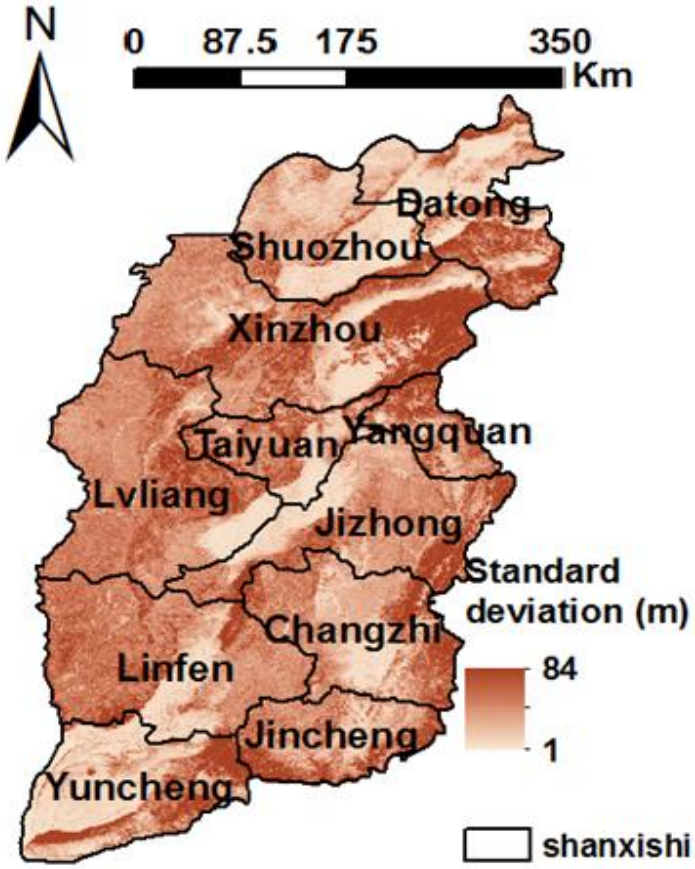

Figure 3. 3 Standard deviation of elevation throughout the study area.

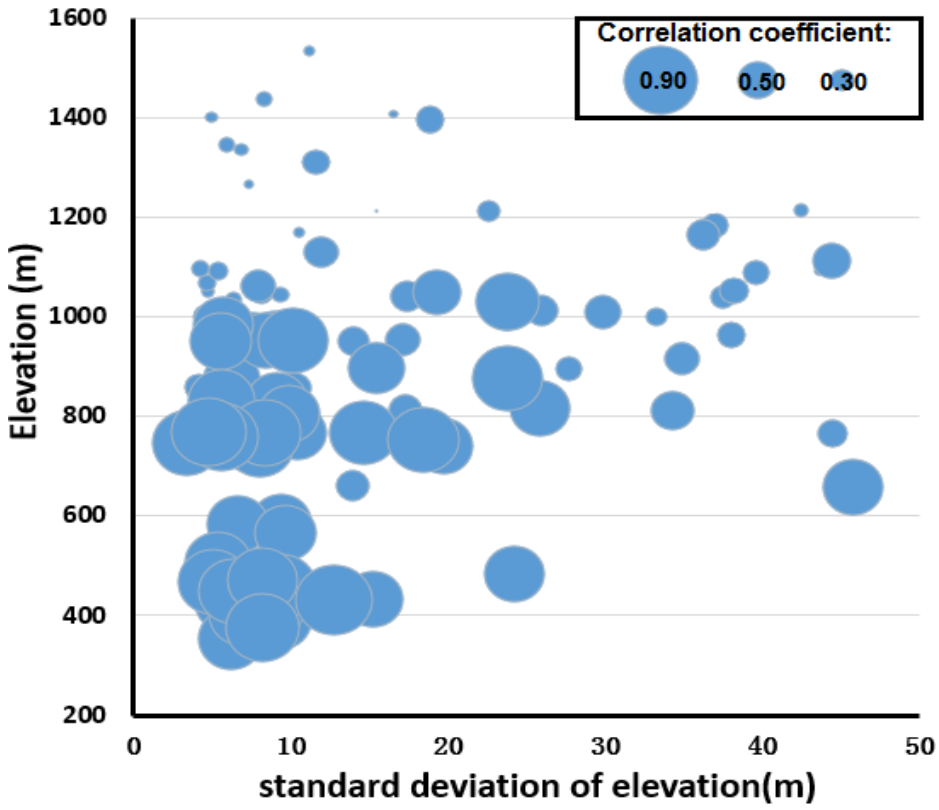

Figure 3. 4 Relation among correlation coefficient, elevation, and standard deviation of elevation at 108 in situ stations.

3.1.2 Land use type

Next we investigate the land use types in Shanxi Province. Figure 3.5 shows the land use map over Shanxi Province in the 2000s, derived from the China 1 km mesh land use dataset. The six major land use types documented in the dataset are forest, grassland, field, rural residence, urban, and water. The western parts of the study area are mostly covered with field. All of the basins (Datong, Taiyuan, Xinding, Changzhi, Linfen, and Yuncheng) are dominated by mixed rural residence and urban. Forest and high coverage grassland are distributed through Changzhi, Jincheng and east of Lvliang. The eastern part of Xinzhou features some grassland. In the northern parts (Datong and Shouzhou), where the land use types were quite mixed, the correlation coefficients between the AMSR-E and in situ soil moisture were as low as 0.3 in 2006 and 2007. Therefore, we consider that land use types also affect the relationship between the two soil-moisture datasets. Conversely, in areas of

single land use (Linfen, Yuncheng, and Changzhi Basins), the correlation coefficients were relatively high (>0.7).

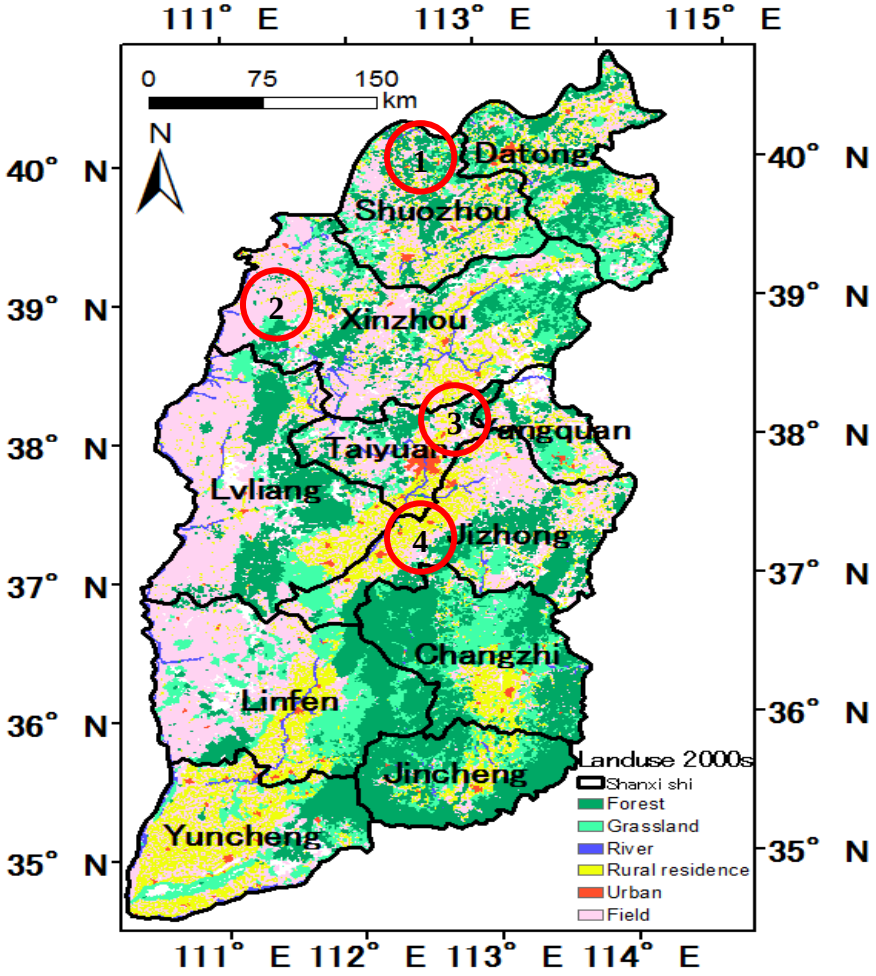

Figure 3. 5 Chinese 1 km mesh land use map of Shanxi Province in the 2000s. Circles enclose four representative areas.

3.1.3 Validation results

The density of the ground-based observation stations varies throughout the study area, as seen in Figure. 3.2. Therefore, we analyzed the correlation coefficients at four representative sites, whose locations are indicated in Figure 3.5. Areas 1 and 2 both host a single in situ observation station and their land use types are uniform. Area 1 is dominated by fields (68% land use), whereas area 2 contains extensive grasslands (56% land use). The wide range in correlation coefficients reflects the different topographical complexities in

the two areas. The standard deviation of the elevation is 27.76 m in Area 1 and 5.94 m in Area 2. Areas 3 and 4 also have the same number of situ observation stations (seven), but the complexities of their topographies are very similar (with elevation standard deviations of 9.86 m and 5.64 m, respectively). Moreover, the land use types are various in Area 3 (30% field, 28% grassland, 39% rural residence and urban, 3% other) but uniform in Area 4. Here, the wide range in correlation coefficients arises from the different land use types in the two areas.

Comparing Areas 2 and 4, both with uniform land use type and similar topographical complexity (5.94 m and 5.64 m, respectively), we observe high correlation coefficients (>0.80) in Area 4 (with seven in situ observation stations), and relatively low correlation coefficient in Area 2 (with only one station). Therefore, when comparing the AMSR-E and ground-based soil moisture, the number of in situ observation stations should be considered. In the study area, the observations are denser in the north (average 5–7 stations per 50 km by 50 km area) than in the south (average 1–2 stations per 50 km by 50 km area). The small station densities at some sites will probably bias the average soil moisture when comparing with AMSR-E data.

As an alternative approach, we also considered the whole of Shanxi Province, and averaged the AMSR-E soil moisture and (separately) in situ soil moisture in all 108 observation stations on each ground-based observation day. For this analysis, we selected only full coverage images, discarding observation days in which the AMSR-E soil moisture did not cover the whole Shanxi Province. The comparison results are presented in Figure. 3.6. The AMRS-E data well agree with the in situ soil measurements (coefficients of determination up to 0.93). Therefore, the soil moisture variability over Shanxi Province is adequately represented by the data from 108 in situ stations). This indicates that as the ground-based observation points become denser, the correlation between the AMSR-E and in situ soil moisture will improve. Low density is probably the most important cause of the

low correlation coefficients (<0.3). We conclude that AMSR-E accurately determines the variation in surface soil moisture when the in situ observation stations are closely spaced. This implies that in the comparison with in situ datasets over Shanxi Province, the accuracy of the AMSR-E soil moisture product is guaranteed.

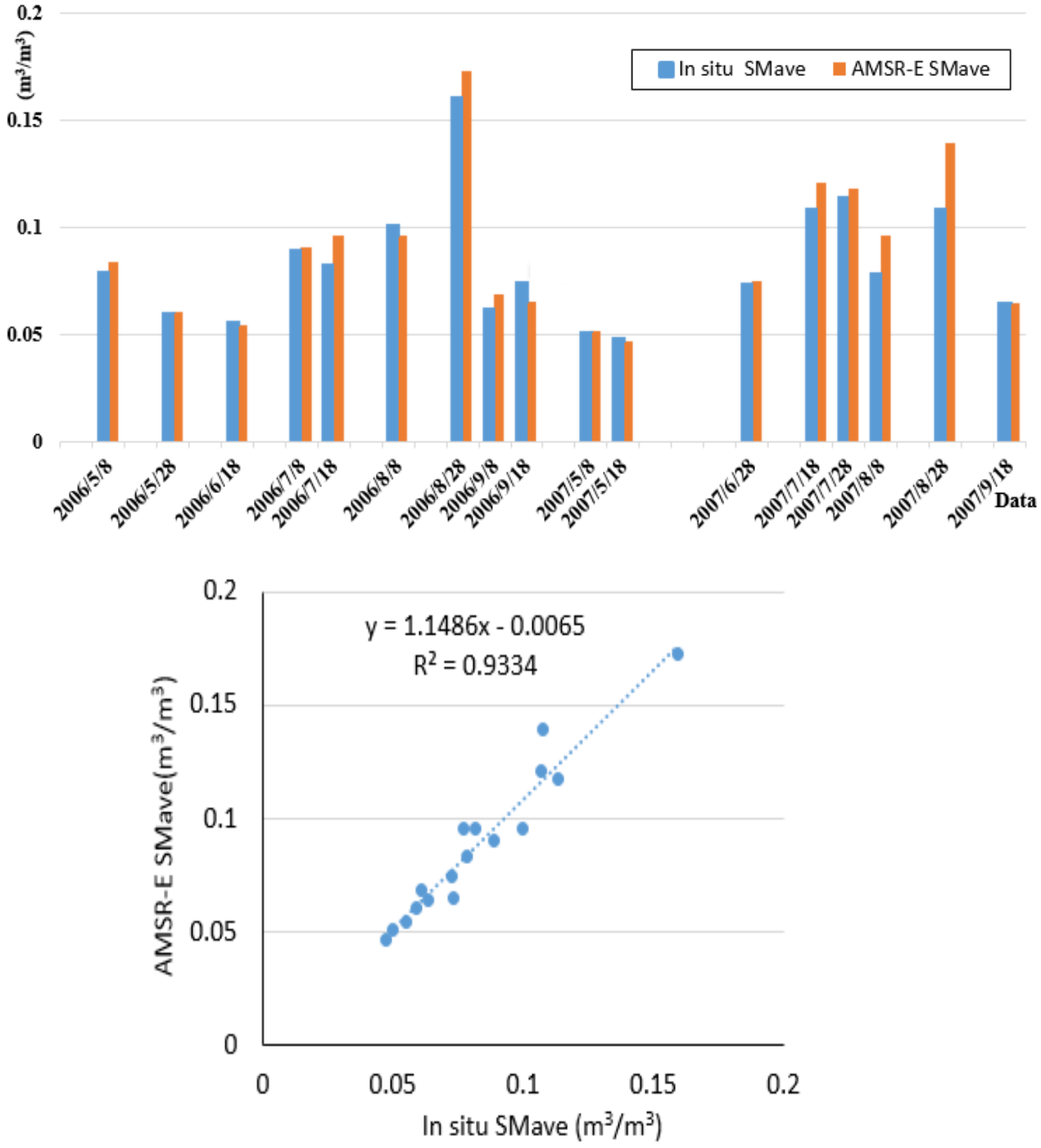

Figure 3. 6 Comparisons between AMSR-E and in situ soil moisture over Shanxi Province (SMave denotes average value of soil moisture).

The 108 in situ observation stations over Shanxi Province differed in their elevations, standard deviations of elevation, average precipitations and land use types. Therefore, after the analysis, we selected five (a–e) representative areas from Datong in the north, Taiyuan and Yangquan Basins in the center, and Linfen and Changzhi Basins in the south. The essential information of each representative area, with a scope of (50 × 50) km^2, is summarized in Table 3.1. Figure 3.7 relates the AMSR-E soil moisture to the in situ soil moisture in the 5 areas. Although the AMRS-E data are sometimes overestimated by around 10%, most of the data scatter near the 1:1 line, indicating good agreement between the two datasets. Kaihotsu et al. (2009) showed that microwaves detect very thin soil layers (depth 1–2 cm) in regions with high water content. On the other hand, in situ soil moisture is averaged over soil depths of 0 to 10 cm. After a rainfall, the AMSR-E data are affected by both surface soil moisture and vegetation surface water, leading to overestimation. The validation results are improved in the no rain periods of the observation time.

Table 3. 1 Characteristics (latitude, longitude, elevation, standard deviation of elevation, annual mean precipitation, and land use) in five representative areas of Shanxi Province.

Code	Name	Lat°	Lon°	Elevation (m)	Std Dev (m)	Pave (mm)	Main land use
a	Datong Xian	40.00	113.60	1023	14	388	Grassland
b	Meng Xian	38.00	113.35	1177	29	482	Forest land
c	Qingxu Xian	37.50	112.35	755	9	470	Field
d	Guandao Kou	36.00	112.88	991	19	631	Grassland
e	Xu Cun	35.75	111.37	456	11	539	Grassland

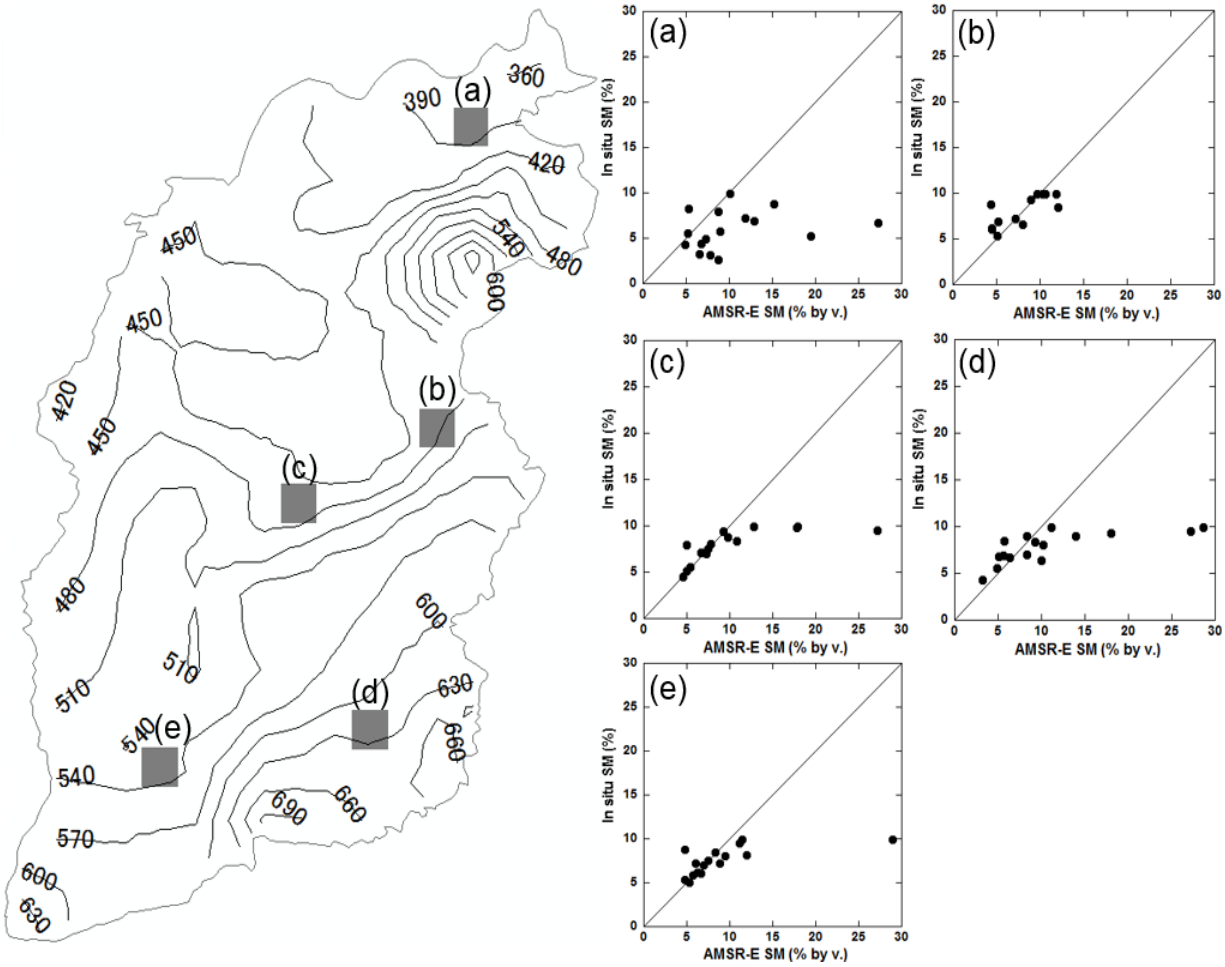

Figure 3. 7 Average annual rainfall and the relations between AMSR-E and in situ soil moisture at five representative areas.

3.2 Spatial and temporal distribution of soil moisture

Above, we confirmed that AMSR-E soil moisture data are applicable to Shanxi Province. In this section, we analyze the spatio-temporal variation of soil moisture over the study area using the AMSR-E data. Figure 3.8 shows the monthly maximum mean soil moisture from April to September over a 7 years period (2003–2009). The soil moisture is low over the entire region in April, then increases from May, reaches its maximum in August and decreases in September. This pattern corresponds to the seasonal changes of precipitation. Spatially, the soil moisture value is low in Datong and Shuozhou, west of Xinzhou, Lvliang and Linfen, and highly variable (0.05–0.6 m^3/m^3) in Changzhi, Jincheng and Yuncheng. Over Shanxi Province, the soil moisture tends to increase from northwest to

southeast, following the annual mean precipitation distribution in Fig. 3.7. Overall, the soil moisture matches the climatological distribution of precipitation. Therefore, AMSR-E is very helpful for estimating surface soil moisture over large regions.

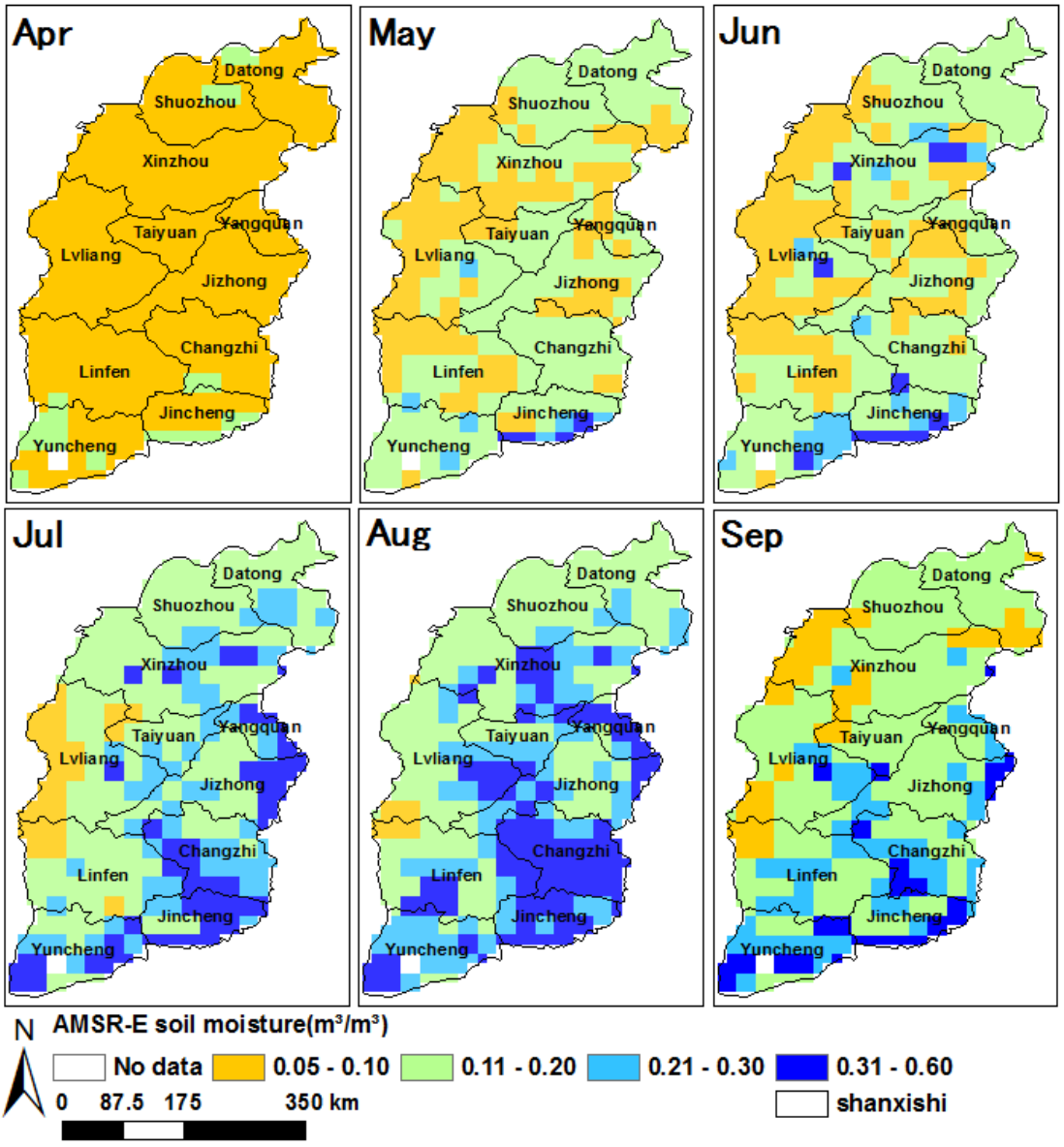

Figure 3. 8 Monthly (April to September) maximum means of AMSR-E soil moisture from 2003 to 2009 with grid size is (30 by 30) km^2.

After analyzing the long-term variation in soil moisture, we plotted the mean AMSR-E soil moisture over the first ten days of July, August and September in 2006 and 2007. Temporally, the soil moisture increases from July to August, then gradually decreases toward September. Spatially, the soil moisture is higher in the south (Yuncheng, Changzhi,

and Jincheng) than in the north (Datong, Shuozhou, and Xinzhou), and higher in the east (Yangquan, Jinzhong, and Changzhi) than in the west (Lvliang and Linfen). Especially, the soil moisture in Yuncheng Basin remained high throughout the observation period. Succinctly, there are good short-term correspondences between the soil moisture collected by AMSR-E and in situ measuring instruments.

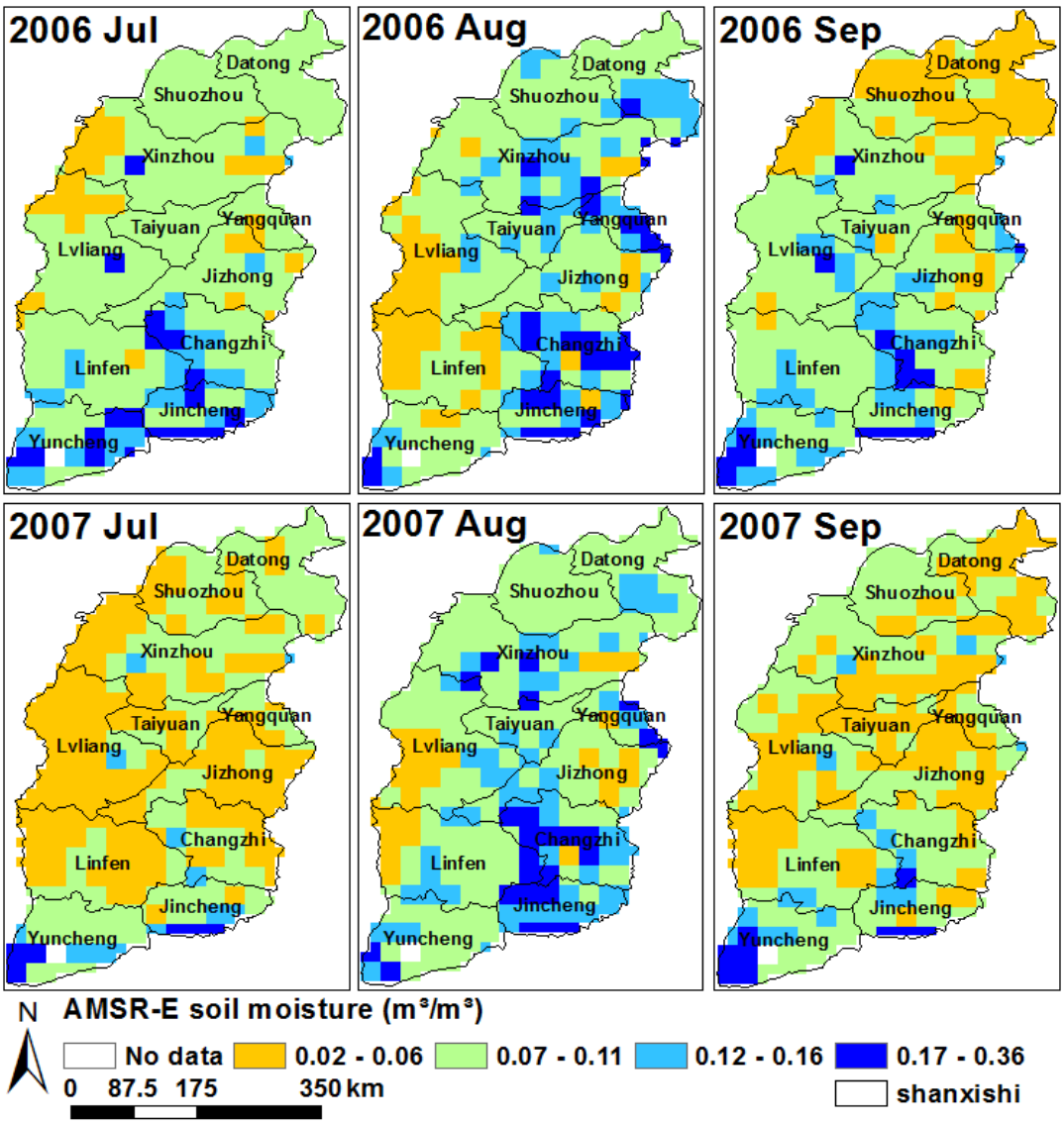

Figure 3. 9 AMSR-E soil moisture averaged over the first ten days of July, August, September in 2006 and 2007 with grid size is (30 × 30) km^2.

Among various parameters, soil moisture is most closely linked to precipitation. Therefore, to understand the variation in AMSR-E soil moisture, we must reveal the rainfall situation of Shanxi Province. The cumulative precipitation throughout the early

tend days of July, August, and September in 2006 and 2007 is shown in Figure 3.10. During July of those years, the rainfall was low (<30 mm) in Taiyuan, Yangquan, and the western part of Xinzhou, but high (>60 mm) in Yuncheng and Jincheng; in August, the rainfall was low in the western parts of Lvliang and Linfen and high in the northern parts (Datong and Shuozhou); in September, the low and high rainfall areas were the northern (Datong, Shuozhou and Xinzhou) and southern (Linfen, Yuncheng) parts, respectively.. Comparing these results with the soil moisture variations (Figure. 3.9) over the same time scale, we find that the AMSR-E soil moisture well corresponds with precipitation. This confirms that the AMSR-E soil moisture captures the wetness of the Earth's surface in APHRODITE's precipitation measurements. However, there are discrepancies in some areas. For instance, during the first 10 days of August in both years (2006 and 2007), the rainfall was low in the southern part (Changzhi and Jincheng) while the soil moisture values were high. However, the soil moisture in this two southern areas were lowered during the middle ten days of August. The main reason for these discrepancies is the different observation timings. Moreover, Yellow River was exploited for agricultural irrigation, as discussed later.

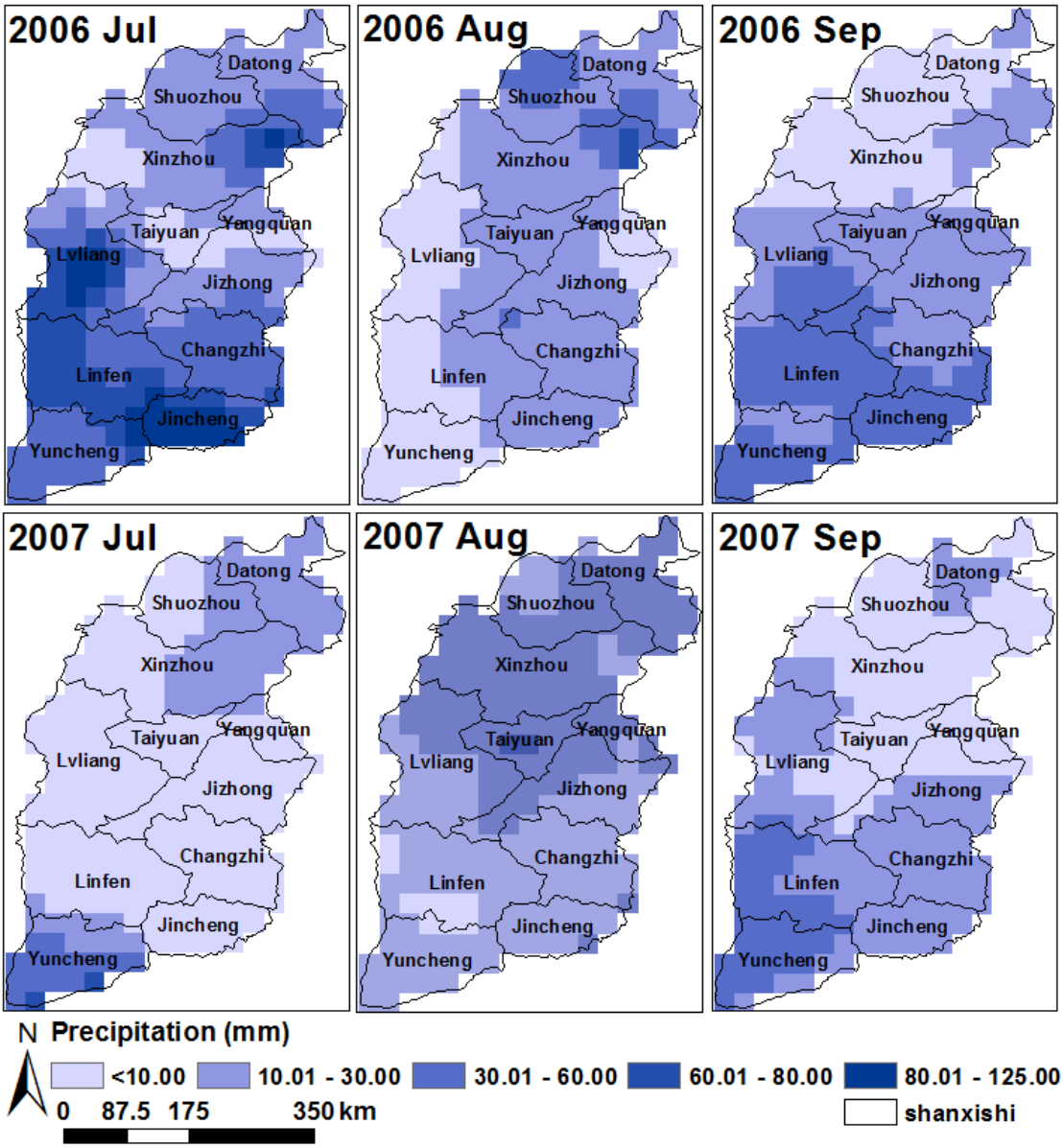

Figure 3. 10 Integrated APHRODITE precipitations over the first ten days of July, August and September in 2006 and 2007.

3.3 Relationship between precipitation and soil moisture

Above we clarified the average annual rainfall over the long-term, and the spatio-temporal variation between soil moisture and APHRODITE precipitation in the early days of July, August and September of 2006 and 2007. In this section, we discuss the relationship between AMSR-E soil moisture and precipitation over short (daily) time scales, and present time series of the AMSR-E soil moisture, in situ soil moisture and precipitation. The analyses are developed in 3.3.1 and 3.3.2, respectively.

3.3.1 Daily changes of precipitation and soil moisture

Daily surface soil moisture, which is closely linked to precipitation, changes excessively in arid and semi-arid region. In such regions, it rapidly increases after a daily rain event, but is rapidly lost by evaporation during the following dry period (Shinoda, 2005). As an example, Figure. 3.11 shows the variation between AMSR-E soil moisture and APHRODITE precipitation on 28th and 29th July 2006. On 28th July, the rainfall and AMSR-E soil moisture were both high in the west of Shuozhou and Xinzhou (18 mm and 0.2 m^3/m^3, respectively), but had rapidly reduced by the next day. On the other hand, the north of Shuozhou, east of Xinzhou and Jincheng were dry on 28th July, but the soil moisture increased after precipitation on 29th July. Comparing the precipitation and AMSR-E soil moisture in regions of high and low soil moisture on 28th and 29th July, we find a strong correspondence, indicating that AMSR-E soil moisture can determine the surface wetness over small spatio-temporal scales.

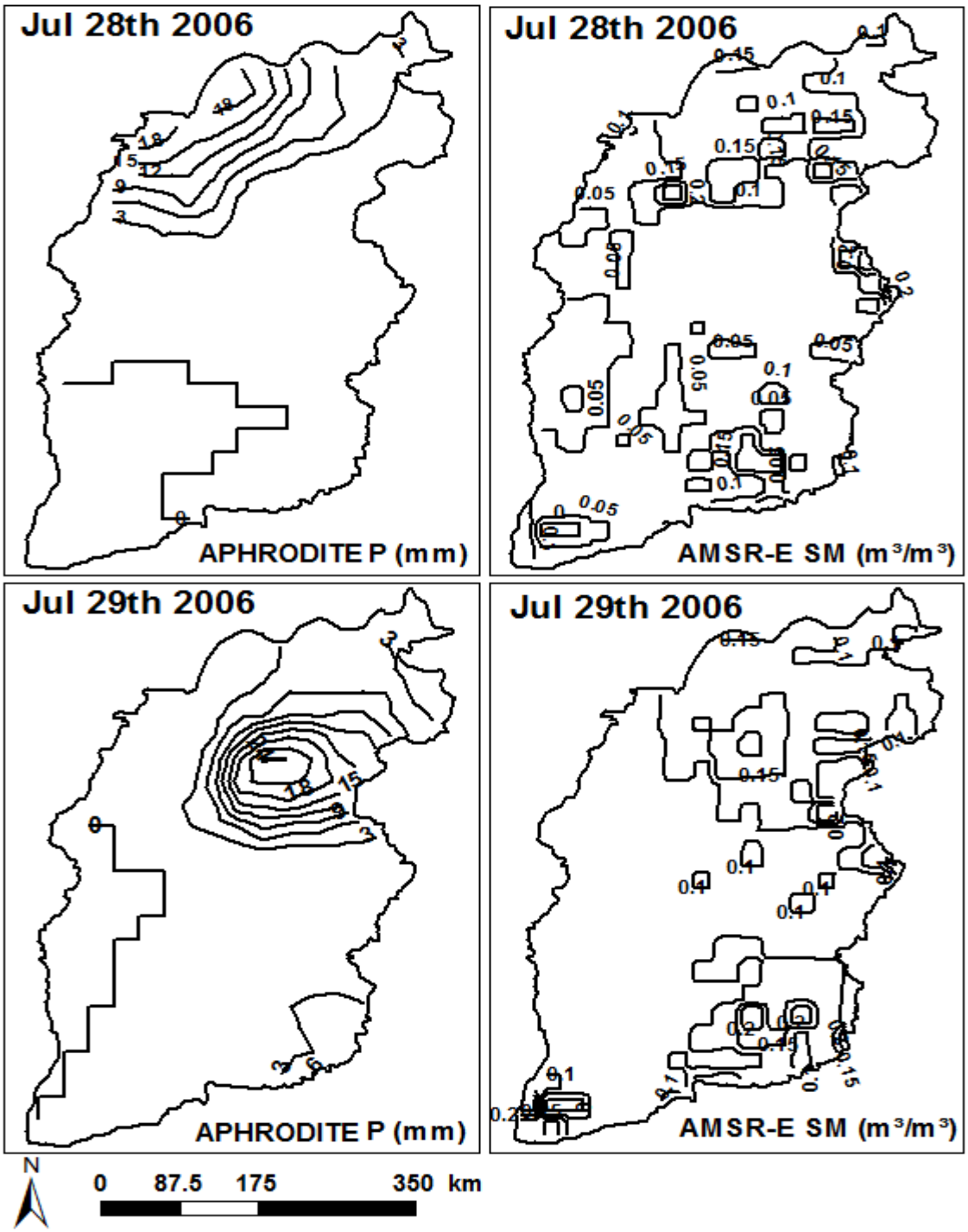

Figure 3. 11 Variation between AMSR-E soil moisture and APHRODITE precipitation on 28th and 29th July 2006.

3.3.2 Time series of precipitation and soil moisture in representative areas

Figure 3.12 presents the time series variation in the AMSR-E soil moisture, in situ soil moisture and precipitation data from April to September in 2006 and 2007 at five representative areas; Datong Xian (a), Meng Xian (b), Qingxu Xian (c), Guandao Kou (d) and Xu Cun (e); see also Table 3.1. Despite some missing data, the precipitation and soil moisture followed the same trends during both years. Their peak values were especially consistent. Although there were significant changes in the AMSR-E soil moisture, the ground-based soil moisture varied very little. Furthermore, the soil moisture content remained nearly constant (at 5%) during periods of no or very low (<5 mm) rainfall. However, after rainfalls exceeding 5 mm, the soil moisture did not always increase, or increased several days later. Considering the special topographical features of water concentration, the time lag scales at each station need further analysis, and is left as a future research topic. When the soil moisture failed to respond to the rainfall, the observation timings of the soil moisture and precipitation were different. Because the AMSR-E soil moisture is instantaneously sampled during the satellite's passage, the daily precipitation can occur before or after the satellite observation time (1:00–2:00 p.m. around the equator). Figure 3.13 highlights the inconsistency between the precipitation and AMSR-E soil moisture in areas (c) and (d). At Qingxu Xian (c), there was low precipitation and high soil moisture on 21th August 2006. Because this area contains crop fields, it is irrigated for crop growth. Therefore, the high surface soil moisture is attributable to agricultural water. At Guandao Kou (d), the summed precipitation was 10.85 mm on 7th August 2006, but the soil moisture content was very low. This suggests a precipitation event after the satellite passage.

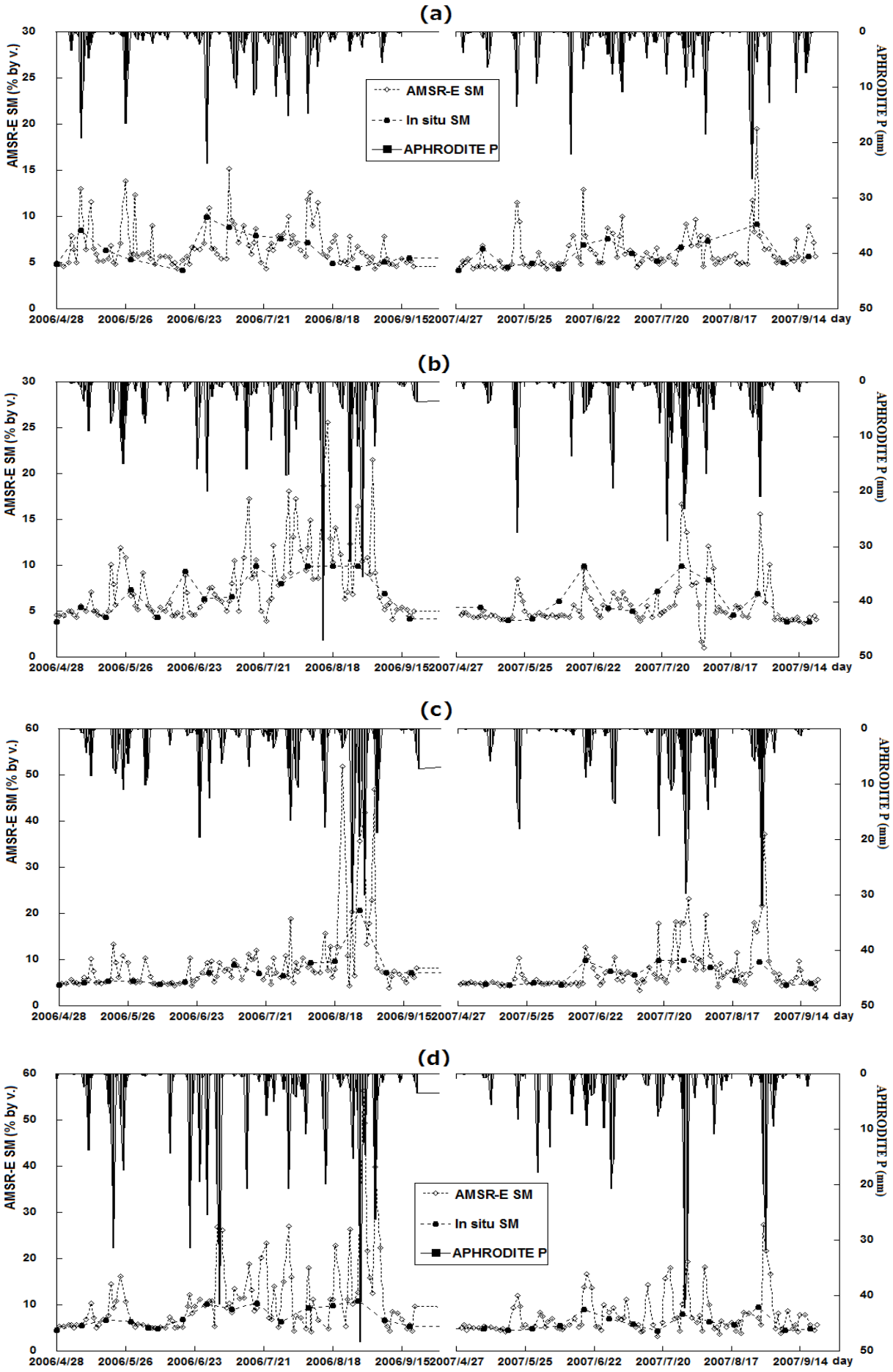
(a)
AMSR-E SM (% by v.)
APHRODITE P (mm)
AMSR-E SM
In situ SM
APHRODITE P
2006/4/28
2006/5/26
2006/6/23
2006/7/21
2006/8/18
2006/9/15
2007/4/27
2007/5/25
2007/6/22
2007/7/20
2007/8/17
2007/9/14
day
(b)
AMSR-E SM (% by v.)
APHRODITE P (mm)
2006/4/28
2006/5/26
2006/6/23
2006/7/21
2006/8/18
2006/9/15
2007/4/27
2007/5/25
2007/6/22
2007/7/20
2007/8/17
2007/9/14
day
(c)
AMSR-E SM (% by v.)
APHRODITE P (mm)
2006/4/28
2006/5/26
2006/6/23
2006/7/21
2006/8/18
2006/9/15
2007/4/27
2007/5/25
2007/6/22
2007/7/20
2007/8/17
2007/9/14
day
(d)
AMSR-E SM (% by v.)
APHRODITE P (mm)
AMSR-E SM
In situ SM
APHRODITE P
2006/4/28
2006/5/26
2006/6/23
2006/7/21
2006/8/18
2006/9/15
2007/4/27
2007/5/25
2007/6/22
2007/7/20
2007/8/17
2007/9/14
day

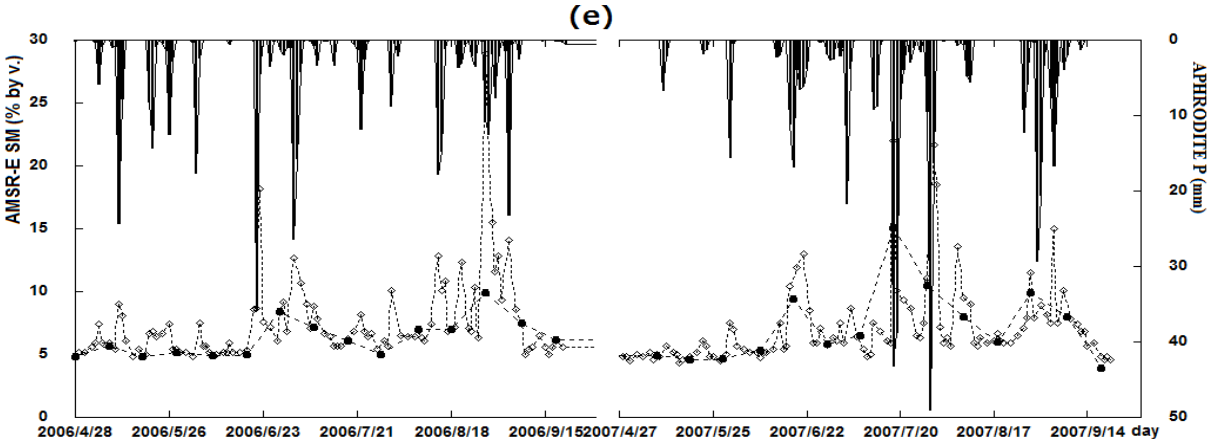

Figure 3. 12 Time series variations in AMSR-E soil moisture, in situ soil moisture and APHRODITE precipitation in five representative areas.

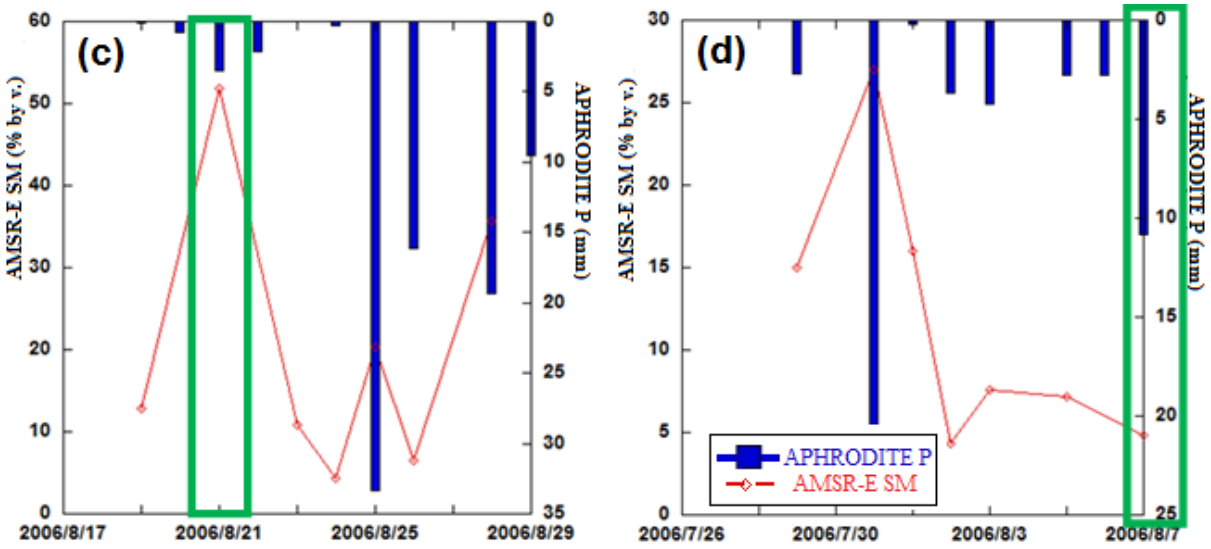

Figure 3. 13 Inconsistencies between APHRODITE precipitation and AMSR-E soil moisture in areas c and d (expanded from Figure. 3.12).

3.4 Relationship between NDVI and soil moisture

The NDVI indirectly affects the vegetation conditions. As the surface vegetation affects the soil moisture, the NDVI should correlate with the soil moisture. This section investigates the spatial and temporal distributions of this relationship, and compares the NDVI and soil moisture at representative areas.

3.4.1 Spatial and temporal distributions of NDVI and soil moisture

Figure 3.14 presents SPOT NDVI images in the early days of July, August, and September in 2006 and 2007. Averaged over all areas, the NDVI increased over the three months, being 0.49, 0.56, and 0.61 in June, July, and August respectively. The NDVI was low in Taiyuan Basin, west of Lvliang, Linfen Basin, and Yuncheng Basin, but high in Changzhi and Jincheng. Following the spatial distribution of the soil moisture (Figure 3.9), the NDVI gradually increased from north to south and from west to east. Nevertheless, the NDVI deviates from the soil moisture at some sites. For example, the eastern part of Lvliang is covered by dense forest and grassland, but the AMSR-E soil moisture was relatively low. Koike *et al*., (2004) suggested that AMSR-E soil moisture is not easily assessed in dense vegetation areas.

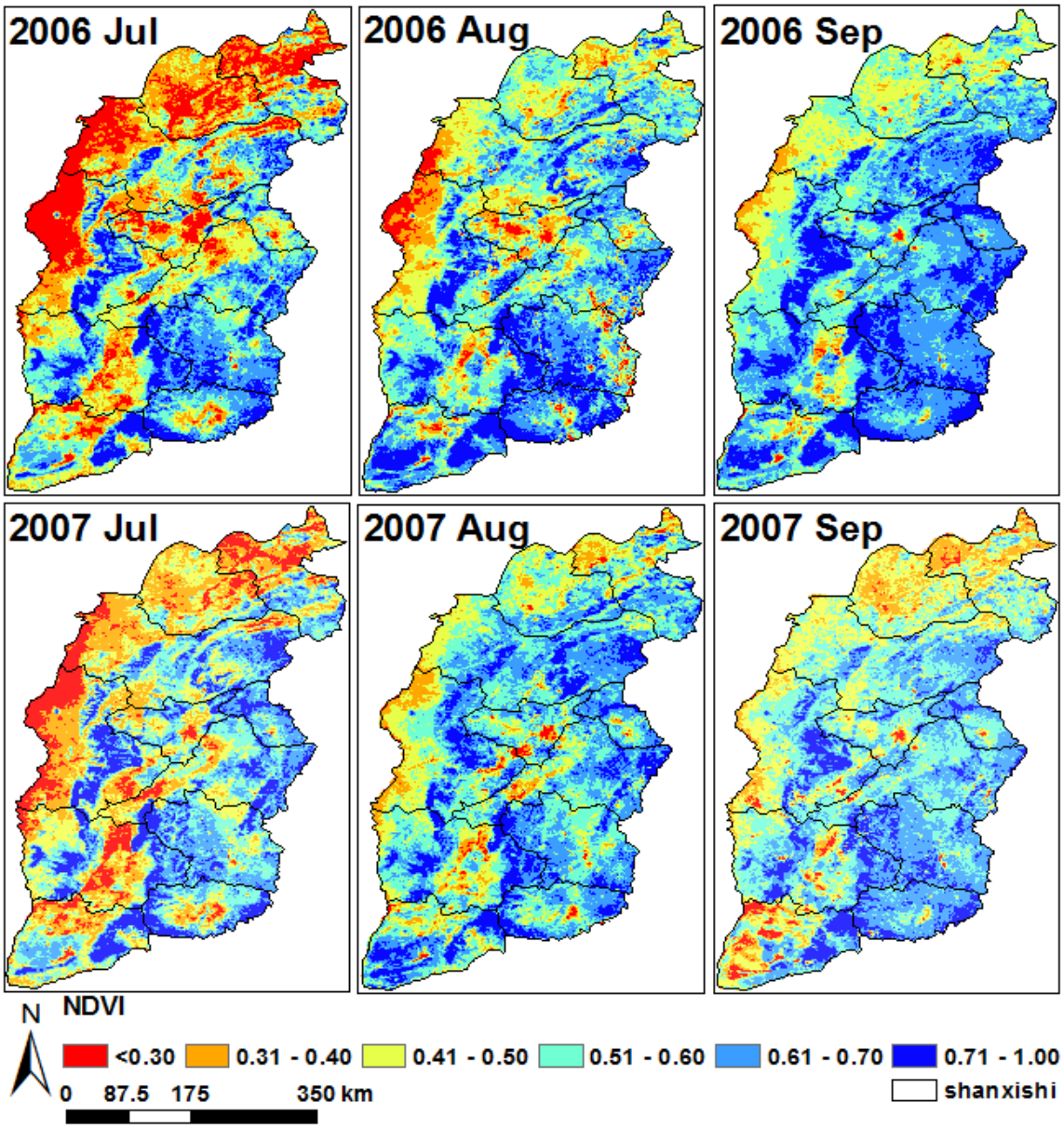

Figure 3. 14 Spatial variation of maximum SPOT/VEGETATION NDVI during the first ten days of July, August, and September in 2006 and 2007.

3.4.2 Comparisons between NDVI and soil moisture in representative areas

Figure 3.15 plots the AMSR-E soil moisture versus NDVI at five representative areas in 2006 and 2007. In Meng Xian (b), where the land use type is forest, the correlation coefficient is high (0.92) and the NDVI is large. The grassland areas Datong Xian (a), Guandao Kou (d) and Xu Cun (e) also exhibit good correlations (correlation coefficients

ranging from 0.67 to 0.78). In Qingxu Xian (c), corn is grown as a main agricultural crop. As the growing season lasts from May to September, the low correlation coefficient (0.41) can be attributed to large changes in NDVI.

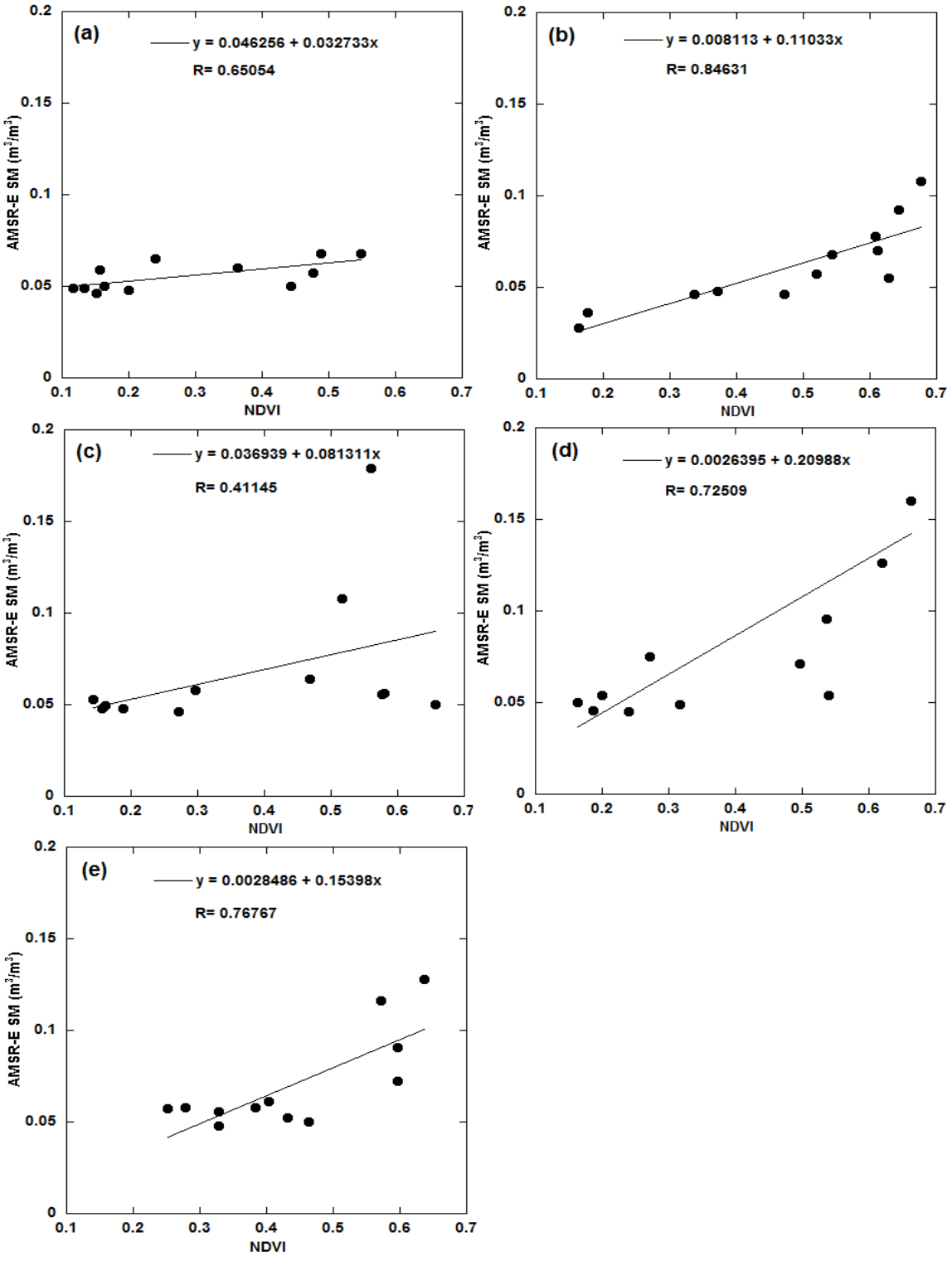

Figure 3. 15 Relationships between AMSR-E soil moisture and NDVI at five representative areas of Shanxi Province.

3.5 Conclusions

This chapter evaluated the AMSR-E soil moisture product (Version.5.31) over the Shanxi Province of China from 28th April to 18th September in two consecutive years (2006 and 2007). In general, the AMSR-E soil moisture product accurately estimated the soil moisture over Shanxi Province. In a correlation analysis between the in situ and satellite datasets, 64 out of 108 ground-based observation points were well or reasonably correlated with the satellite data (correlation coefficients > 0.5). This result demonstrates the high accuracy of AMSR-E soil moisture estimation. During the 2-year study epoch, high correlation coefficients (>0.7) were found over Taiyuan Basin in the central study region, Linfen Basin, Yuncheng Basin, Changzhi Basin, and Jincheng in the south, and the Yangquan areas in the east. Low values (>0.3) were found in the northern parts (Datong and Shuozhou). Values between 0.3 and 0.7 were recognized as moderate correlations. Next, we identified a positive relationship between the correlation coefficients and number of in situ observation stations. However, for the same density of in situ observation stations, the correlation coefficients ranged from large to small. To understand the reason for this variability, we analyzed the topographic complexity and land use types in Shanxi Province. Comparing the in situ and AMSR-E soil moisture at specific sites, we found good agreement between the two datasets in areas of uniform land use type and relatively flat terrain. In two areas with uniform land use types and similar topographic complexities, high and low correlation coefficients were associated with dense (7) and sparse (1) in situ observation stations, respectively. Although the topographic complexity and land use types influence the correlation coefficients to some extent, the main influencer in the northern mountainous areas appears to be the low density of in situ sites (average 1–2 per (50 × 50) km^2 area).

Furthermore, when considering Shanxi Province as a whole element, the daily average AMSR-E soil moisture was well matched with the daily averages of the 108 in situ soil

moisture observations. The correlation coefficient of this analysis was very high (0.93), but could be further improved by densifying the in situ observation stations as much as possible (enabling a proper validation). The low correlation coefficient areas were attributed to the small number of in situ observation stations. It was recommended that more ground-based stations, especially in regions of heterogeneous land use type and complex terrain, be erected for future research. The daily distribution of the AMSR-E soil moisture also agreed with the daily precipitation in the north of Shanxi Province, where there are heterogeneous land use types and complex terrains.

In summer, the large variations and spatio-temporal distributions of the AMSR-E soil moisture were associated with seasonal changes in the APHRODITE precipitation measurements. Furthermore, the surface wetness increased from the northwest to the southeast of Shanxi Province. These two results verified that AMSR-E soil moisture can correctly capture the surface wetness conditions over this large region.

On all time scales (daily, monthly, and annual) and over all spatial distributions, the AMSR-E soil moisture responded to the APHRODITE precipitation in Shanxi Province. Furthermore, the time series variations in the AMSR-E soil moisture, in situ soil moisture and precipitation data were reasonably well synchronized in five representative areas. However, the observation times and recording depths differed between the AMSR-E soil moisture and the APHRODITE precipitations. The AMSR-E soil moisture was instantaneously observed when the satellite passed over the area. In contrast, the APHRODITE instrument summed the daily precipitation. Therefore, if the precipitation occurred after the satellite overpass, the AMSR-E soil moisture would likely remain low while the APHRODITE precipitation increased. Another notable aspect was the limited depth inspection capability of AMSR-E (0–5 mm below the land surface). When the land was irrigated (disturbed by human activity), the land surface was covered with water and the AMSR-E soil moisture was likely to be overestimated. For these reasons, the AMSR-E

soil moisture was sometimes inconsistent with the APHRODITE precipitation.

Across the study area, the spatial and temporal distributions of the AMSR-E soil moisture were reasonably related to the vegetation index (NDVI). The correlation between these two variables was high in areas covered by vegetation. However, the AMSR-E soil moisture was difficult to assess in dense forest areas. The relationship between AMSR-E derived soil moisture and NDVI in areas with many vegetative species should be explored in future research.

In this chapter, we investigated the AMSR-E soil moisture in Shanxi Province of China, and related them to the land and climate variables. Using these findings, we characterize the soil moisture distributions and variations in flat areas (middle and lower Yangtze River plain and Sichuan Basin) of East Asia over daily, monthly and annual scales in the next chapter. This work is connected to the applicability of the AMSR-E data.

Chapter Ⅳ. Spatio-temporal characteristics of soil moisture in East Asia

This chapter describes an application of the AMSR-E soil moisture. In Chapter III, the accuracy of the AMSR-E soil moisture was confirmed on areas of flat terrain and uniform land use. Using these findings and features of the AMSR-E soil moisture in Shanxi Province, we now characterize the soil moisture distribution and variation in two representative flat areas of East Asia (the middle and lower Yangtze River Plain and Sichuan Basin). In the first two sections, we investigate the daily, monthly, and annual time scales of the soil moisture; in the third section, we clarify the soil moisture distributions and variation features over the whole of East Asia, taking the monthly averages of seven years. The fourth section presents time-series comparisons between AMSR-E soil moisture and precipitation in a humid, arid and semi-arid region from 2003 to 2007, which are connected to soil moisture memory. These results reveal the spatial and temporal variations in the soil moisture.

4.1 Regional investigation of the middle and lower Yangtze River Plain

The middle and lower Yangtze River Plain is situated near the southeast of China (Figure 4.1), with latitude 24–35° N and longitude 108–123° E. The region experiences a subtropical humid monsoon climate, with high temperatures and much rainfall in summer, and warm temperatures and low rainfall in winter. The average temperature of most cold months is about 0° C. The rainy season is an important component of precipitation in this region. It starts from late May in the north of Hunan Province, moves to Yangtze River, and arrives at Jiangsu Province early in July. The rainy season is characterized by high frequency and large volume of precipitation, and high relative humidity. The duration of a typical rainy season is 20–30 days (Ren *et al.*, 1986). The bottom panel of Figure. 4.1

shows the complex terrain of this area, which is the flatness of the land (the standard deviation of elevation is less than 10 m almost everywhere).

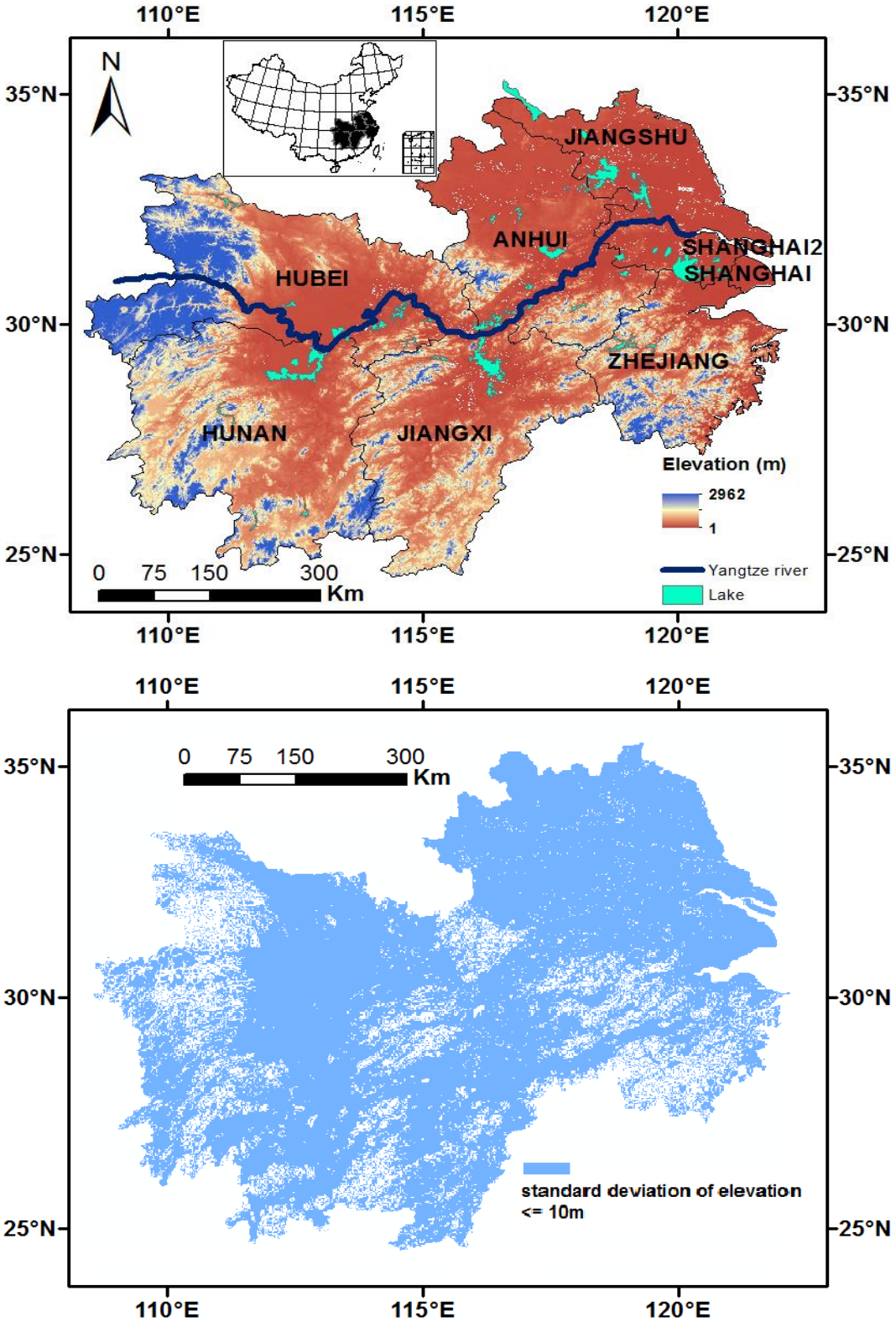

Figure 4.1 Overview of middle and lower Yangtze River Plain (upper panel is an elevation map of the study area; in the lower panel, the standard deviation of elevation is < 10 m, indicating flat terrain).

To understand the soil moisture changes, we first check the daily-scale distribution and variation of the soil moisture in the middle and lower Yangtze River Plain. Figure 4.2 shows the daily variation of the AMSR-E soil moisture and precipitation at Bengbu (32°52′ N, 117°23′ E) near Huaihe River from June to July of 2003. In June, the precipitation was maintained at 10 mm/day, increasing to more than 20 mm/day by the end of the month. Accordingly, the AMSR-E soil moisture exceeded 0.4 m^3/m^3 at the end of June. In July, there were two rainfall events; one lasting from 30 June to 2 July, the other from 8–10 July. Over the three consecutive days of the first and second rainfall events, the total precipitation was 123 mm and 158 mm, respectively. On the other hand, the book *Huaihe Storm and Flood* (published in 2003) recording flooding at Bengbu after the continuous July rains. Other flood information was reported on China's weather news. As shown in Figure. 4.2, the soil moisture follows the same pattern as the precipitation. After a large quantity of rainfall, the soil moisture remained as high as 0.6 m^3/m^3 until mid-July. After a large rainfall, the surface soil moisture remains high and stable over a short time. Therefore, after a large short-term precipitation, the soil moisture in the middle and lower Yangtze River Plain would remain high for several days. The AMSR-E soil moisture in this area ranged from zero to 0.6 m^3/m^3. The maximum AMSR-E soil moisture (0.6 m^3/m^3) may underestimate the real soil moisture, which is maximized under the soil saturation conditions.

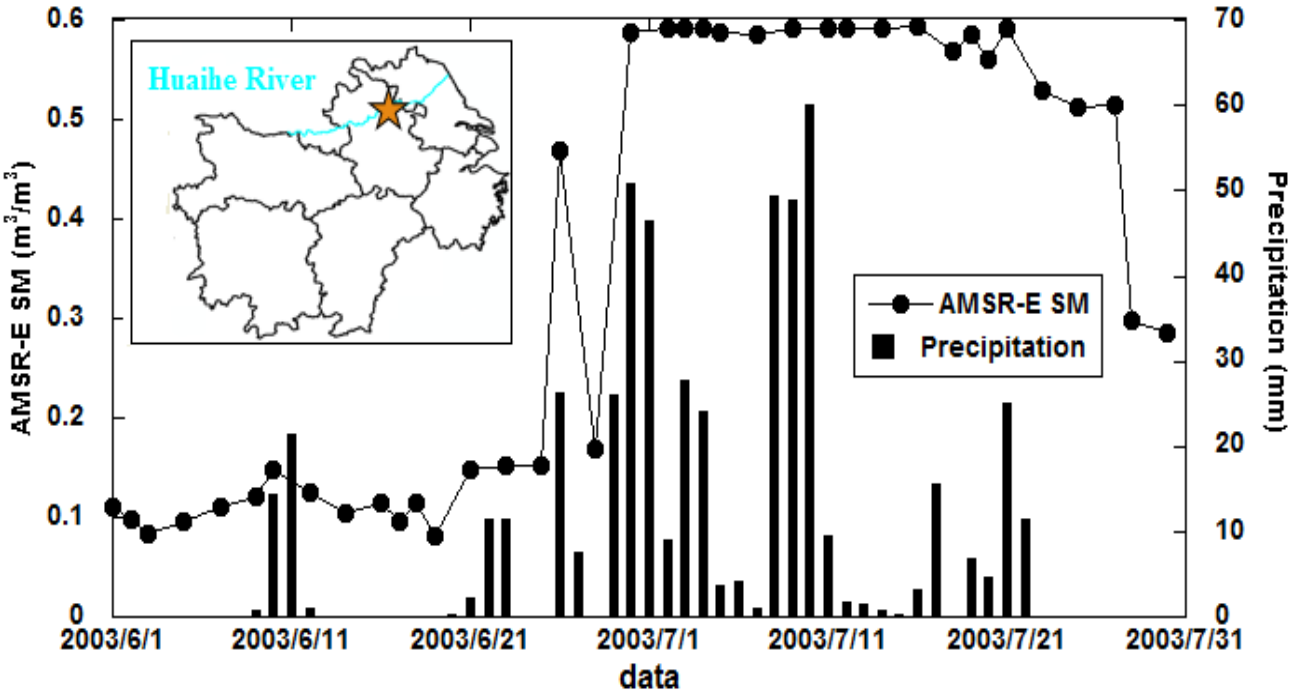

Figure 4.2 Daily changes of AMSR-E soil moisture and precipitation from June to July in 2003 at Bengbu (32°52′N, 117°23′E) near Huaihe River.

Satellite images from Landsat 7 ETM confirmed a flood area near Huaihe River until July 30 of 2003. Therefore, the unique subtropical humid monsoon climate (precipitation) is largely responsible for the soil moisture variation in the middle and lower Yangtze River Plain. The variable AMSR-E soil moisture can capture the flood records, which can be input to weather forecasting models in future research.

As another example, Fig. 4.3 shows the daily weather map and soil moisture distribution in the middle and lower Yangtze River Plain in June and July of 2005. The five left panels represent the 9 a.m. weather maps on the 6th, 20th, and 28th June, and on the 6th and 15th of July 2005, obtained from the Japan Meteorological Agency. The Baiu front gradually moved from south to north over the five time scales. It was located in the south of Yangtze River on 5th June, moved northward through 20–28 June, and remained in the north of Yangtze River through 6–15 July. The five right panels present the AMSR-E soil moisture distributions on the same dates. Like the precipitation, the soil moisture gradually moved from south to north of the middle and lower Yangtze River Plain during June and July. The

soil moisture distribution and the track of the Baiu front exhibit the same tendencies over time. In general, the AMSR-E soil moisture well matches the movement of the rainy season. In this analysis, the weather maps on the 6th and 21st June show no front near Yangtze River, but the Baiu front can be readily tracked in the weather maps of 5th and 20th June.

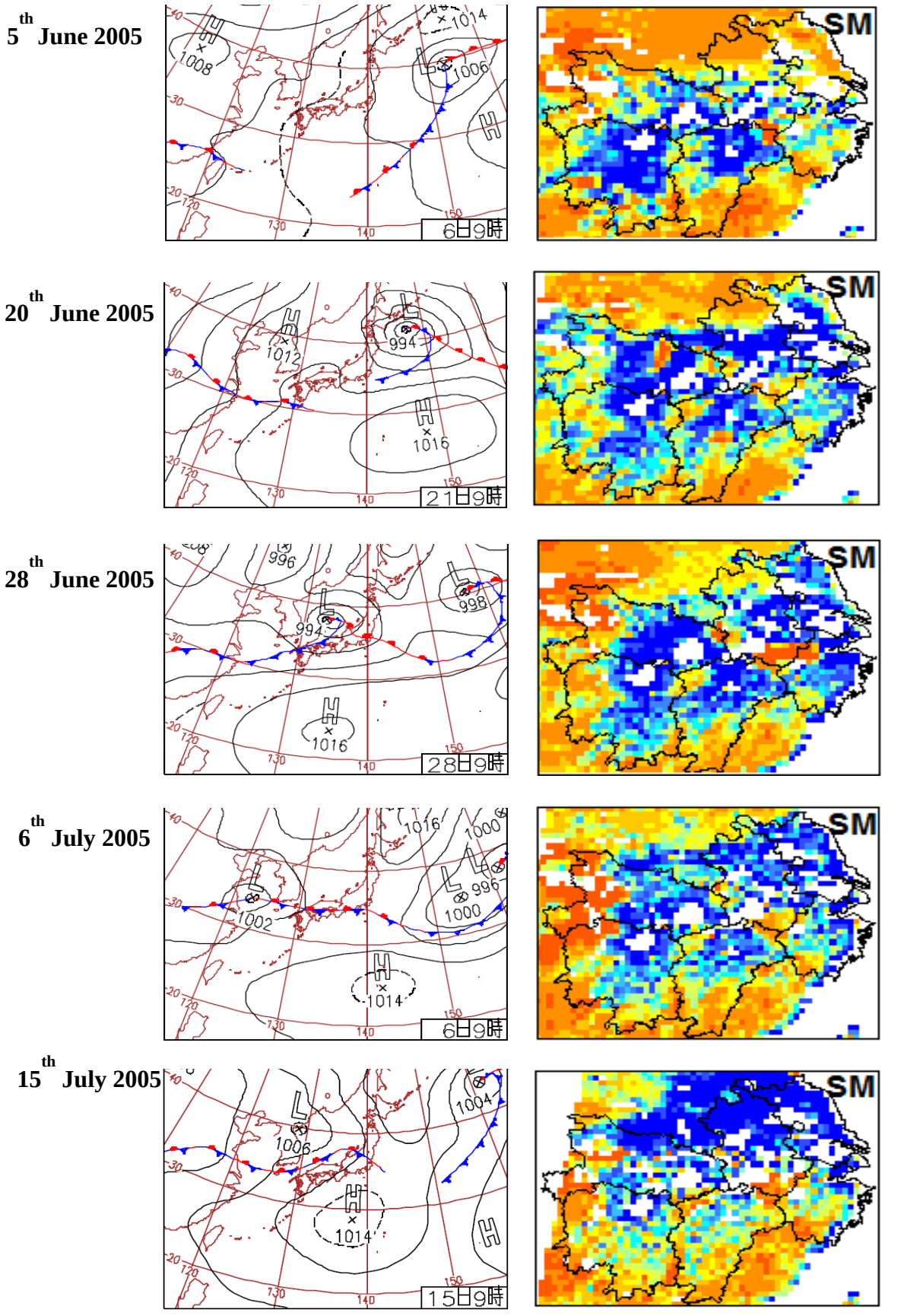

Figure 4.3 Weather maps (black lines are isobars, and H and L denote anticyclone and depression, respectively. Blue lines with triangles and semicircles represent the

Baiu front. Right panels show the soil moisture distributions in the middle and lower Yangtze River Plain on the corresponding dates of the weather maps (5th, 26th, 28th June, 6th, 15th July, 2005).

In this area, the soil moisture is chiefly affected by the humid monsoon climate (precipitation) in the middle and lower Yangtze River Plain. We now check the AMSR-E soil moisture distribution and variation over monthly and annual scales. Figure 4.4 shows the monthly mean AMSR-E soil moisture in the middle and lower Yangtze River Plain from 2003 to 2009. The soil moisture remained high (ranging from 0.06 to 0.10 m^3/m^3 even in winter, with a tendency to increase from March to September and decrease from October to February.

Obvious changes in the soil moisture, with a peak in July, appear around Yangtze River. No data were available for the Yangtze River its tributary and the surrounding lakes (black areas in Figure. 4.4; see also Figure. 4.1). The soil moisture is larger near these areas than in other areas. For example, there was high soil moisture content adjacent to Doting Lake of Hunan Province and Poyang Lake in Jiangxi Province. In August, the soil moisture suddenly declined in the north of Anhui and Jiangsu Province. According to the monthly mean precipitation in this region (Fig. 4.5), the southern part of the middle and lower Yangtze River Plain received large rainfall in May and June. In July, high precipitation appears in the north, revealing the track of the rainy season from south to north. Once the rainy season had passed, the soil moisture rapidly decreased in the north of Anhui and Jiangsu Provinces in August. Therefore, the location of the Baiu front affects the soil moisture changes in different months. The AMSR-E soil moisture is consistent with the precipitation distribution in the middle and lower Yangtze River Plain.

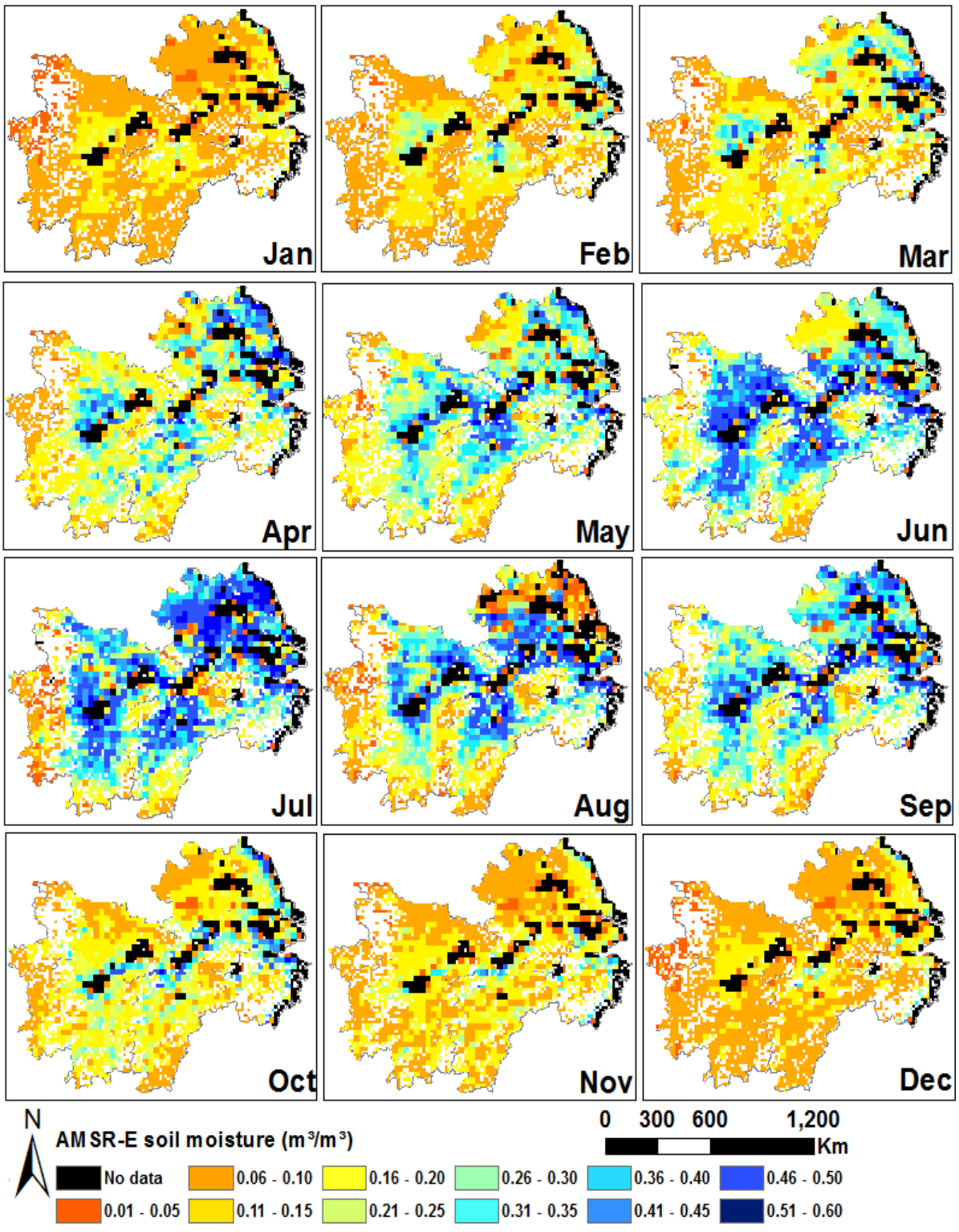

Figure 4.4 Monthly mean AMSR-E soil moisture in the middle and lower Yangtze River Plain from 2003 to 2009.

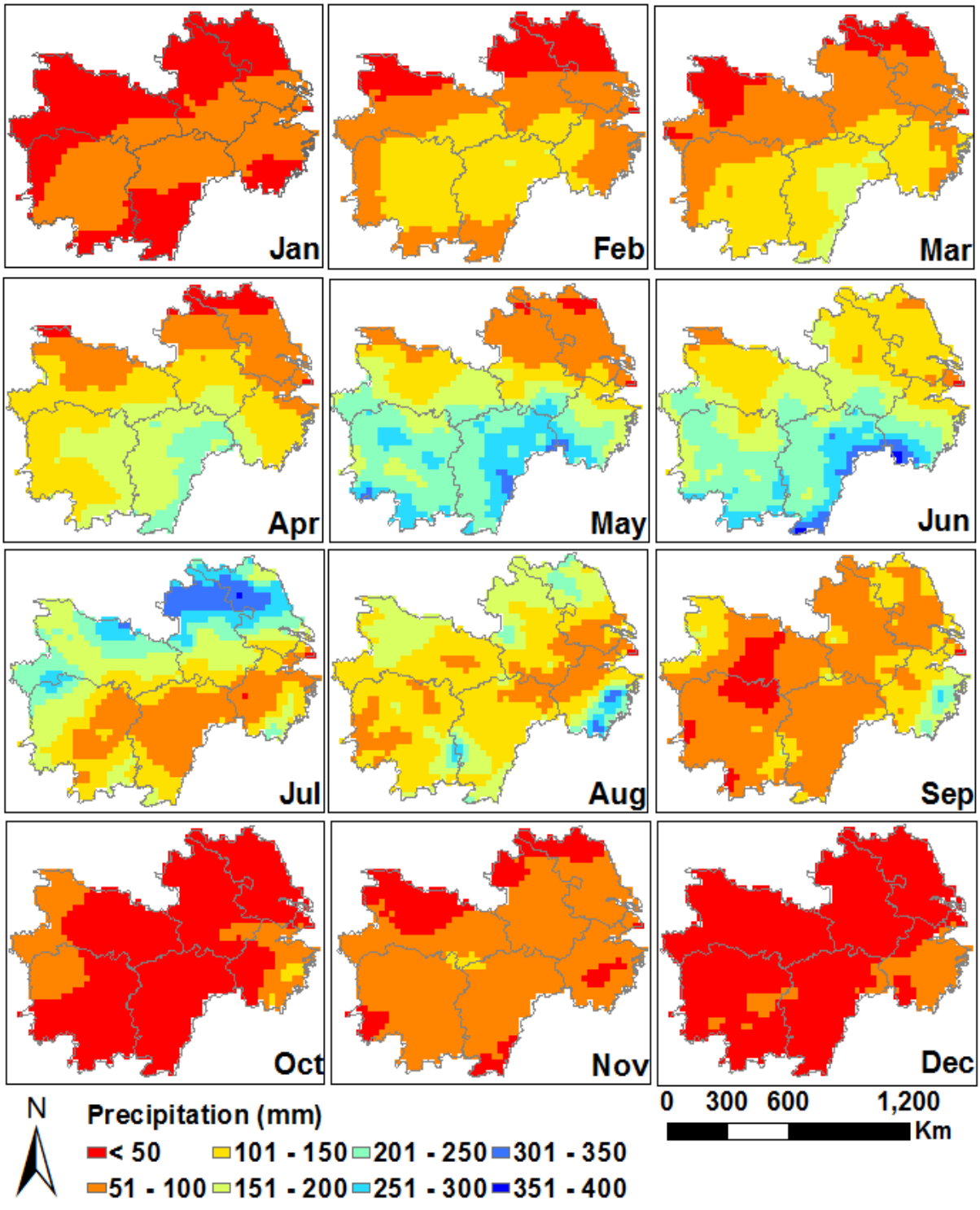

Figure 4.5 Monthly mean precipitation in the middle and lower Yangtze River Plain from 2003 to 2007.

4.2 Regional investigation of Sichuan Basin

Sichuan Province is located in the southwest of China, at latitudes and longitudes of 26–34° N latitude and 92–108° E, respectively. The elevation is high (7000 m) in the west and low (50 m) in the east (see Fig. 4.6). The east of Sichuan Province hosts the relatively flat Sichuan Basin, one of the four largest basins in China and famous for its rice cultivation. There are three distinct features of this region. First, the area is characterized by warm winters (average January temperatures of 2–4° C) and long summers (4.5 months, with maximum temperatures above 40° C in most places). Second, because of the basin topography, many days throughout the year are covered with cloud and fog. Under such conditions, the surface soil moisture is more effectively inferred by the passive microwave sensor of AMSR-E than by an optical sensor. Third, the surface soil comprises purple red sandstone and shale deposits from the Mesozoic period. Sichuan Basin has a subtropical humid monsoon climate, with an annual mean precipitation of 1000–1300 mm.

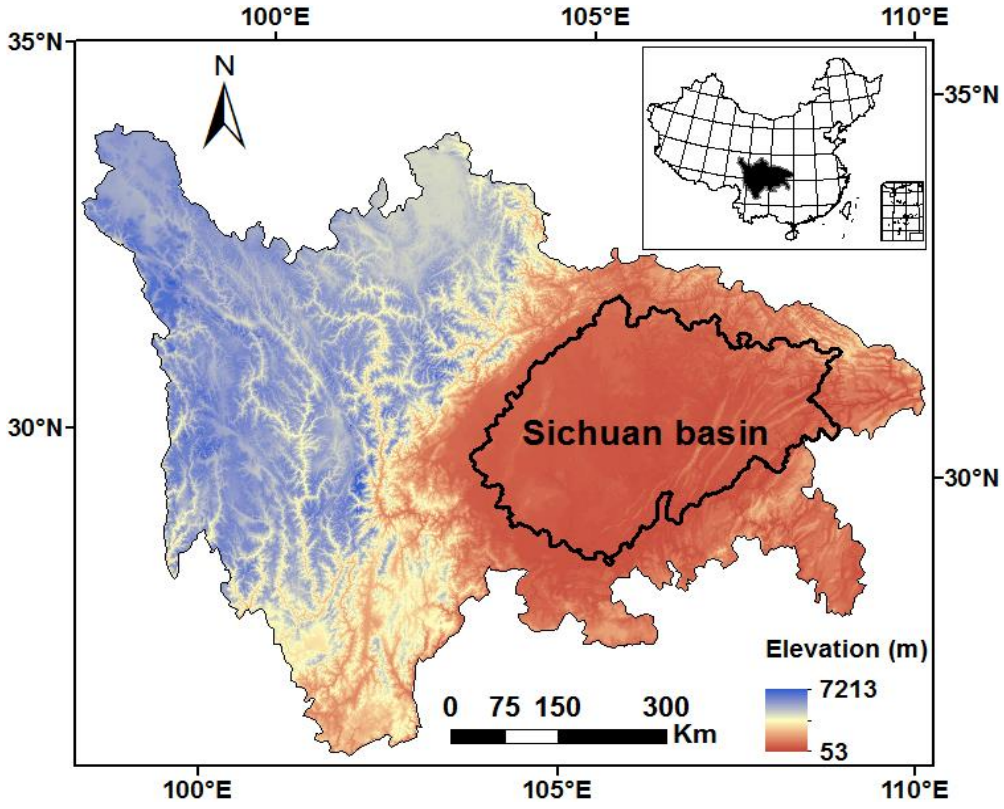

Figure 4. 6 Overview of Sichuan Province.

Although Sichuan Basin occupies the same latitude and climate zone as the middle and lower Yangtze River Plain, its soil moisture variations and distribution are distinctly different.

Sichuan Basin is famous for its rice cultivation. We are interested in the land use of this area, because land use types reflect the topographical features and influence the spatio-temporal characteristics of the surface soil moisture distribution. Figure 4.7 shows the land use of Sichuan Province in the 2000s. The eastern part of Sichuan Basin is dominated by cultivated fields (paddies and fields), whereas the western and edge parts are covered with forest and shrubs. The agricultural crops on the paddies (rice) and fields (corn and wheat), revealed in the land use map of Sichuan Basin, should be closely linked to the soil moisture fluctuations in this region.

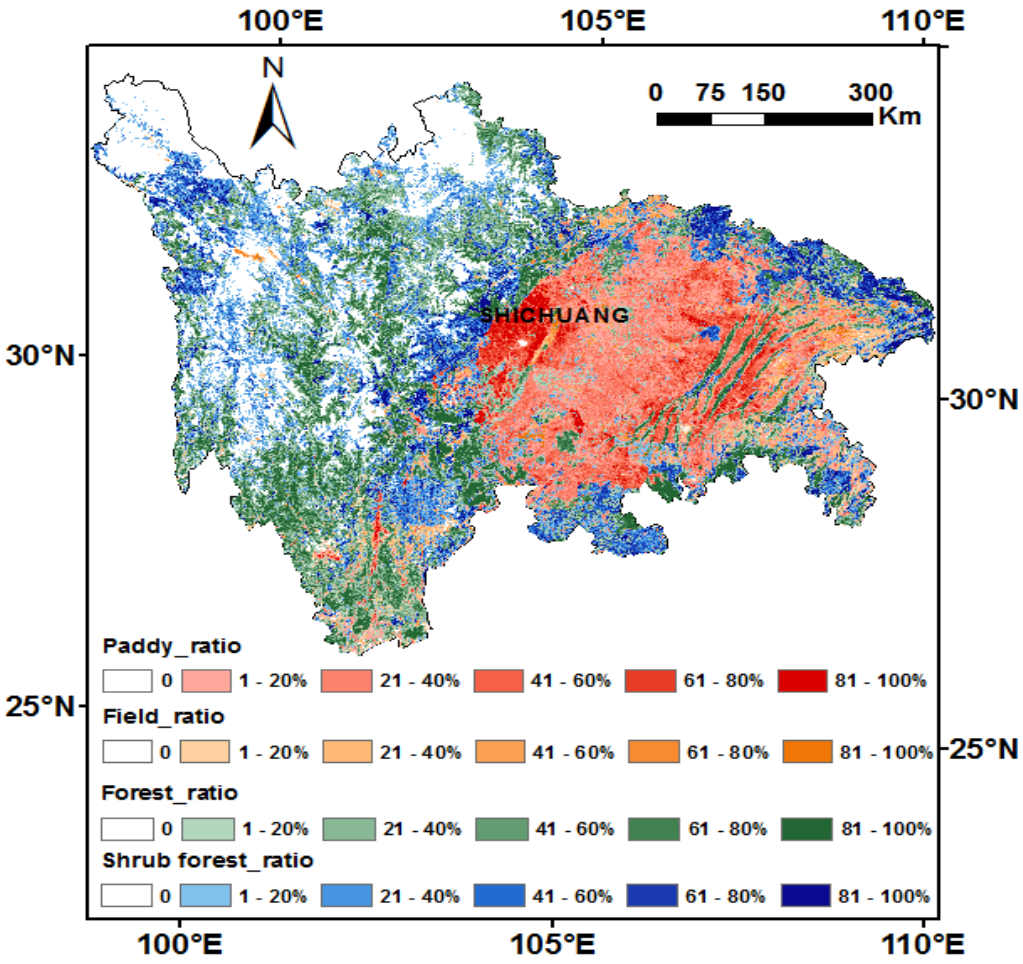

Figure 4. 7 Land use of Sichuan Province in the 2000s.

To reveal the relationship between agricultural crops and soil moisture variation, we extracted the characteristics of the soil moisture in the paddy areas. Figure 4.8 shows the extraction results of the soil moisture on a paddy area in 2006. The soil moisture was stable from January to the end of April and from November to December, but peaked during May and October (green curves in Fig. 4.8). The 2006 time series of SPOT NDVIs in the paddy area is presented in Fig. 4.9. The NDVIs were highly variable throughout the year, with frequent large changes and no obvious peaks. This graph cannot reflect the true growing conditions of paddy in Sichuan Basin, which are affected by the weather situation (cloud). However, as microwave remote sensing can penetrate cloud, haze, and dust, AMSR-E provides more accurate soil moisture information at the land surface than optical sensors.

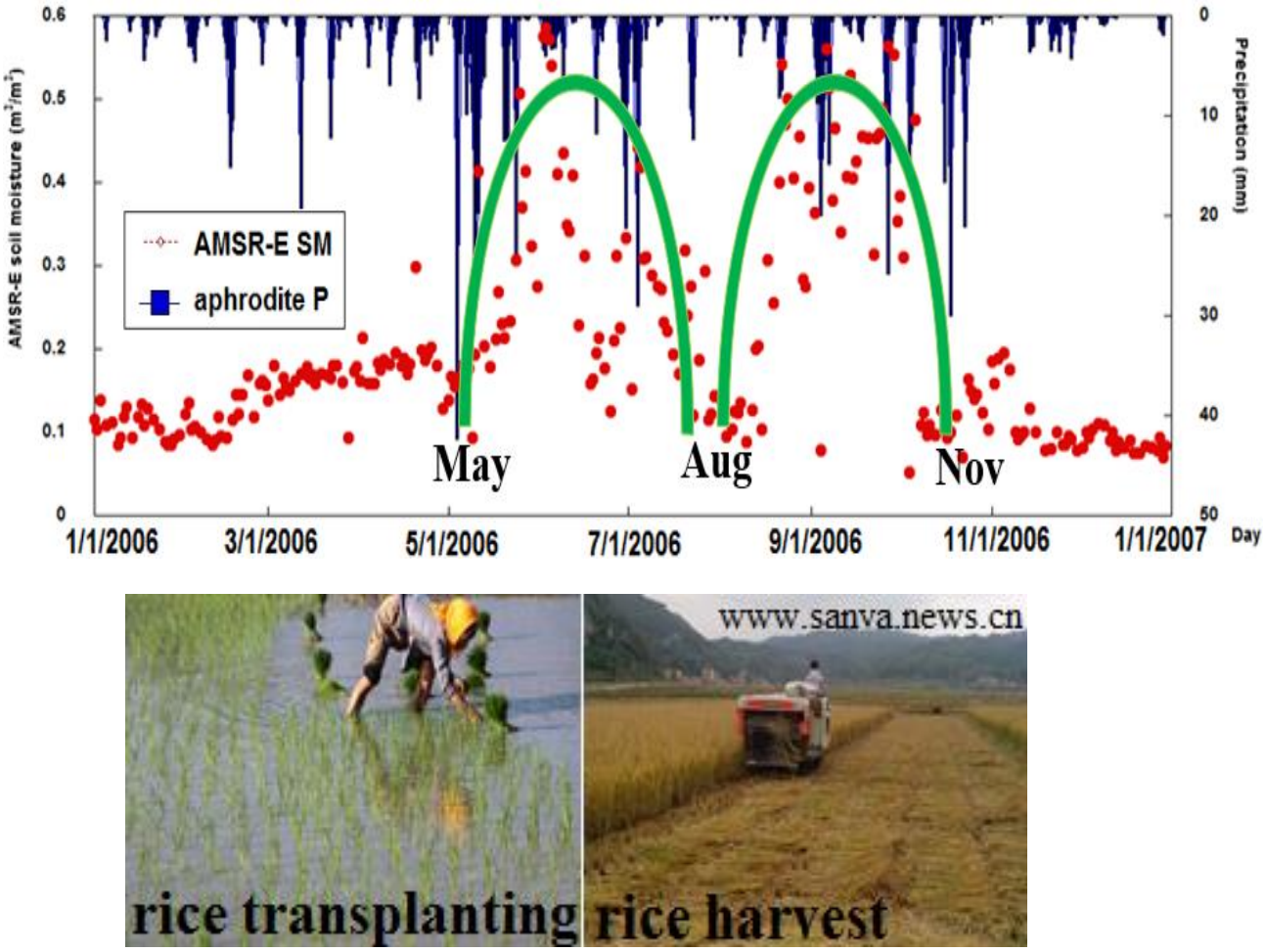

Figure 4.8 AMSR-E soil moisture patterns in a paddy of Sichuan Basin in 2006 (top) and views of rice transplanting and rice harvesting seasons (bottom).

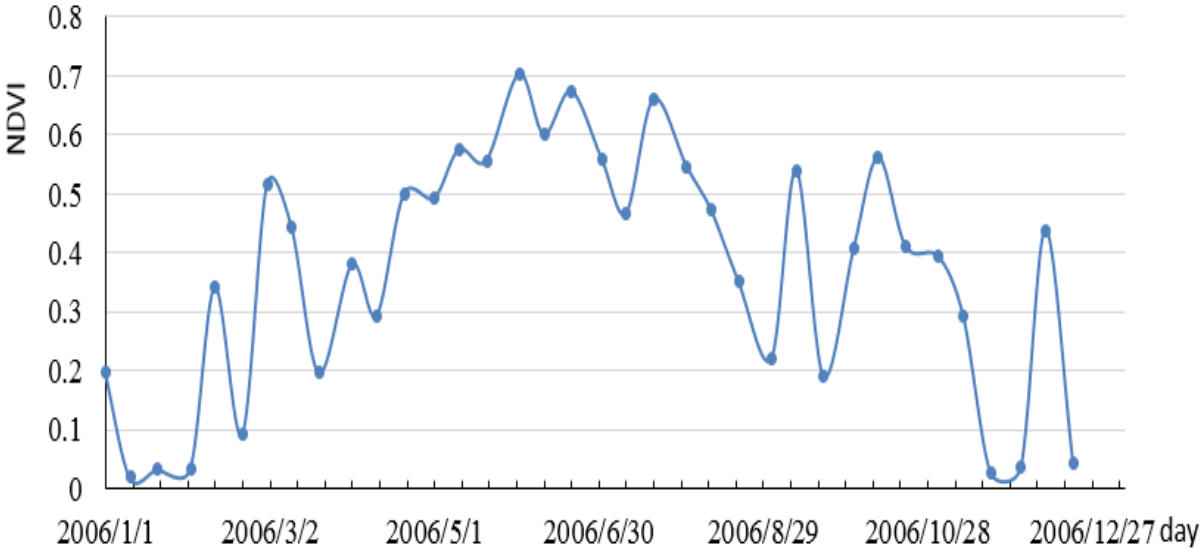

Figure 4.9 2006 time series of SPOT NDVI in a paddy of Sichuan Basin.

In the farming calendar, rice is doubly cropped in Sichuan Basin and its growth cycle is approximately 100 days. After completion of the first rice harvest, the second rice transplanting is performed as soon as possible (Sun *et al.*, 2013). During the rice transplanting seasons (May and August), irrigation is necessary for crop growth. The irrigated land surface is covered with water, so the surface soil moisture increases in May and August. After canopy closure (July and October), the soil moisture begins to decrease. This is a new and important discovery of this research. In summary, the daily AMRS-E soil moisture on paddy areas of Sichuan Basin are influenced by human activity (irrigation), and the variations can be compared with the farming calendar of rice cultivation in Sichuan Basin.

Figure 4.10 shows the monthly mean AMSR-E soil moisture in Sichuan Basin from 2003 to 2009. The soil moisture content remained high over the basin even in winter (>0.06 m^3/m^3), and large variations (~0.45 m^3/m^3) occurred from April to October. The soil moisture continually increased from January to May, remained high in June and July, and declined in August. The average soil moisture over the southern Sichuan Basin exhibited the same growth tendency up to September, but decreased from October to December.

To evaluate the effects of precipitation on soil moisture, we calculated the variation in the monthly mean precipitation (Fig. 4.11). As the APHRODITE precipitation dataset terminated in 2007, we present the time series of the monthly mean precipitation from 2003 to 2007. In winter, the precipitation was small (<30 mm) over the whole area. In spring and autumn, it was higher in the east than in the west. However, no regular precipitation distribution was observed in summer. The AMSR-E soil moisture distribution was not directly related to precipitation in this area. For example, the northern part of Sichuan Basin receives large rainfall in July, but the soil moisture is high at the west of the basin. Therefore, precipitation does not decisively affect the soil moisture distribution in Sichuan Basin. As mentioned previously, in production areas of main food crops, surface soil moisture is influenced by both precipitation and irrigation. The same results are observed on Sanjiang Plain, an important paddy field in the northeast of China.

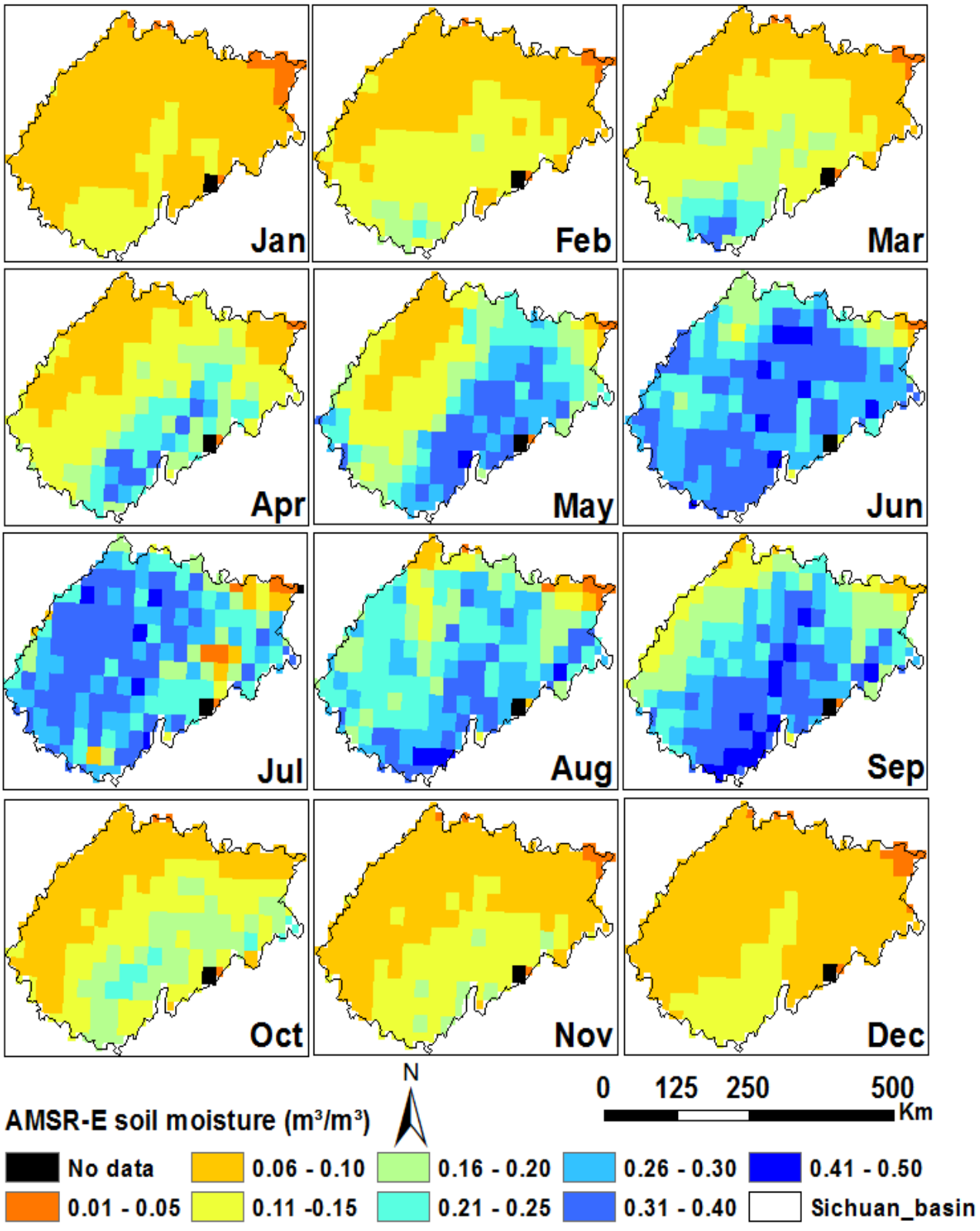

Figure 4. 10 Monthly mean AMSR-E soil moisture in Sichuan Basin from 2003 to 2009.

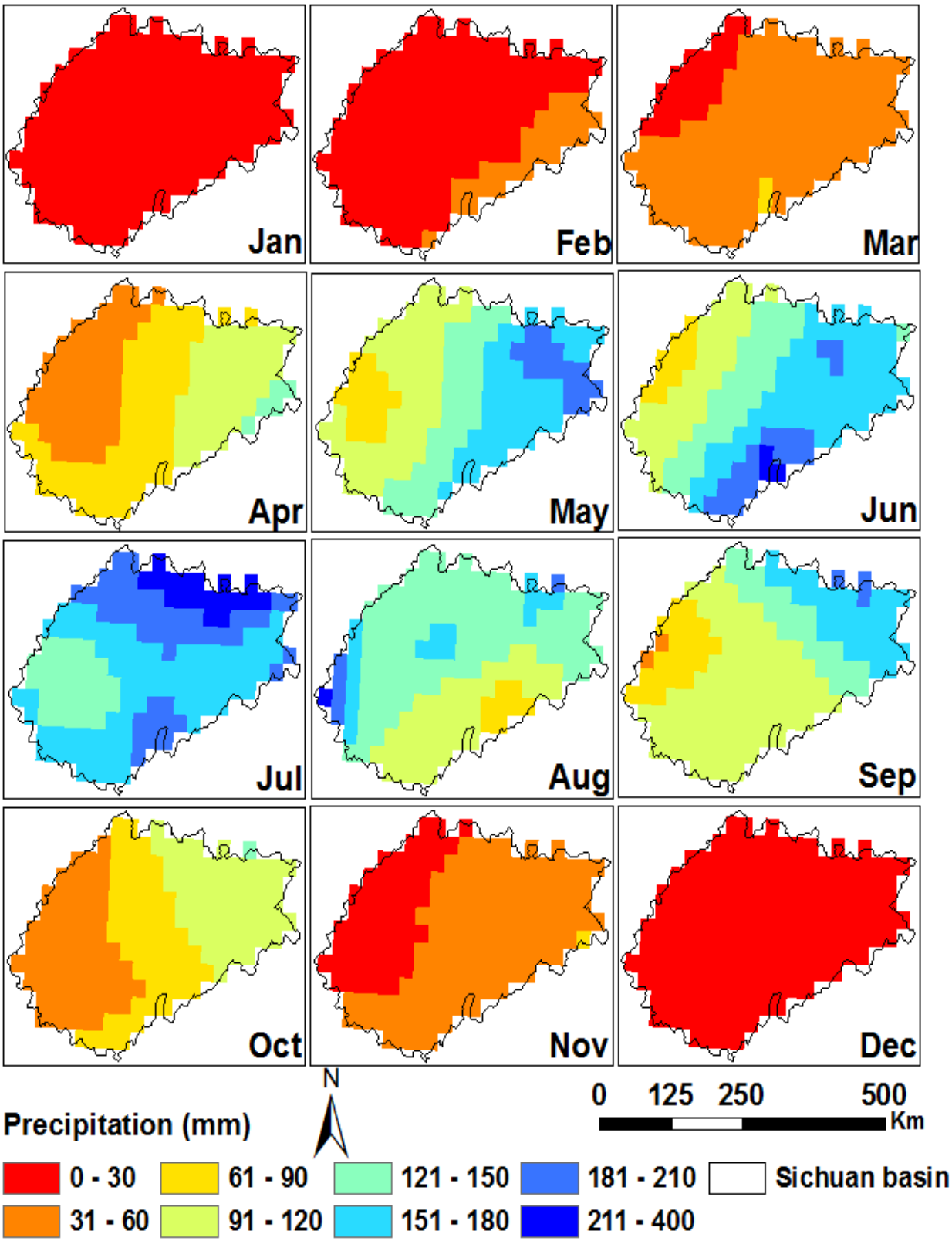

Figure 4. 11 Monthly mean precipitation in Sichuan Basin from 2003 to 2007.

4.3 Distribution and variation features of soil moisture in East Asia

Based on the validation results in Shanxi Province, this section analyzes the soil moisture in representative regions of East Asia. The analysis is limited to the available observation scope of AMSR-E (20–50°N and 72–136° E). Figure 4.12 shows the monthly (May to September) mean AMSR-E soil moisture from 2003 to 2009. At a glance, the soil moisture is high in the east coastal region of East Asia, and low in the west continental region. To characterize the soil moisture changes, we separate the whole area into the following regions:

Northeast of China (Heilongjiang Province, Jilin Province, and Liaoning Province): In May, the soil moisture maintain low everywhere except the eastern Sanjiang Plain and the western Northeast Plain. In both of these areas, the soil moisture increases in June. Although there are missing data in some parts, both plains present a high soil moisture content. The average soil moisture decreases in August and increases in September, for reasons which will be discussed later.

North China Plain (Beijing, Tianjin, Hebei Province, Henan Province, and Shandong Province): The soil moisture in this region remains stable throughout May and June, and increases from July to September, particularly in Shandong Province.

Middle and lower Yangtze River areas (Hunan Province, Hubei Province, Jiangxi Province, Anhui Province, Jiangsu Province, Zhejiang Province and Shanghai): This region is a relatively humid area with high AMSR-E soil moisture throughout the year. Even in winter, the soil moisture exceeds 0.06 m^3/m^3 at least, and summer values are as high as 0.6 m^3/m^3 in some areas.

Southeast coastal hills (Guangdong Province, Guangxi Province, and Fujian Province): Soil moisture varies more widely in coastal regions than in the inland region of southern China. In Guangdong and Guangxi Provinces, the soil moisture fluctuates largely in both coastal and inland regions. Unusually, the soil moisture in Fujian Province are stable

everywhere except the coastal areas.

Mongolian plateau (Inner Mongolia and Outer Mongolia): The average elevation of this region is 1580 meters. The soil moisture obviously varies from east to west and from south to north from June to September.

The loess plateau (Shanxi Province, Shaanxi Province, and Ningxia): This area contains semi-arid and arid terrains. In August and September, the soil moisture is more variable in Shaanxi Province than in other areas. In June, small variations appear in the southeast of Shanxi Province, as detailed in the previous chapter.

Yungui plateau (Yunnan Province and Guizhou Province): The soil moisture in Guizhou Province varies slightly throughout the whole year.

Tibetan plateau (Qinghai Province and Tibet): At a glance, we observe many black areas of no data collection in Figure. 4.12, which correspond to lakes. One of the biggest lakes (Qinghai Lake) is located in Qinghai Province. The soil moisture varies more widely around the lakes than in other regions.

Others areas (Sichuan Basin, Xinjiang, and Gansu Province): Sichuan Basin, located in the east of Sichuan Province, presented clear variations in the average AMSR-E soil moisture. In contrast, the soil moisture in Xinjiang and Gansu Province regions showed little monthly variation, but slightly varied over a long north-to-south distance, as they were influenced by other factors.

Russian areas (southern Russia only): The northernmost part of the study area (the Siberian region) is characterized by cold weather conditions. In some areas, the soil moisture begins increasing from May, remains high throughout the next three months, and then rapidly declines in September.

West of Japan (Kyushu, Shikoku, Chugoku, and part of Kansai): In contrast to the inland region of China, the AMSR-E soil moisture remain high in west Japan throughout the year. The same soil moisture pattern appears in Taiwan.

Indo-Gangetic plain (India and Bangladesh): A striking contrast appears between the northern and southern sides of the Himalayan Ranges. In Bangladesh, the soil moisture peaks (at 0.6 m^3/m^3) from May to September. On account of these regional characteristics, significant spatio-temporal changes in soil moisture present over the large region.

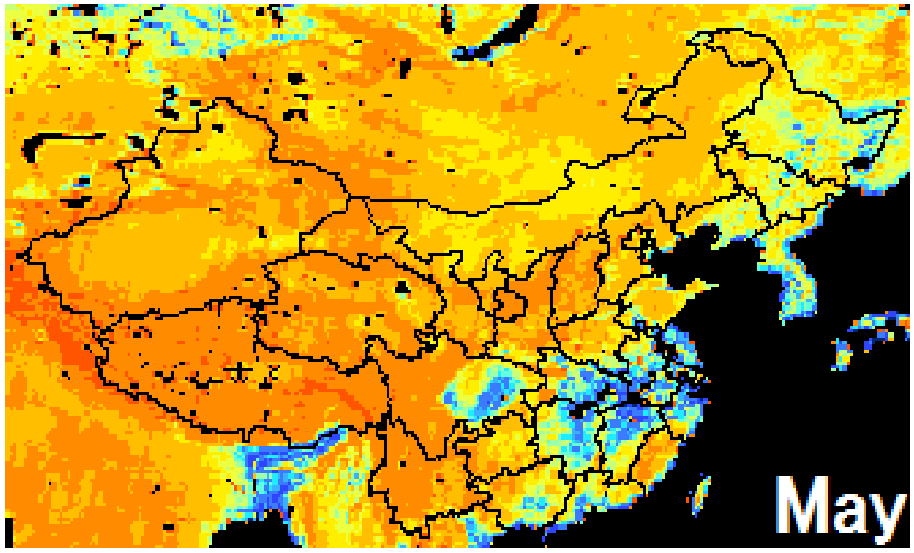

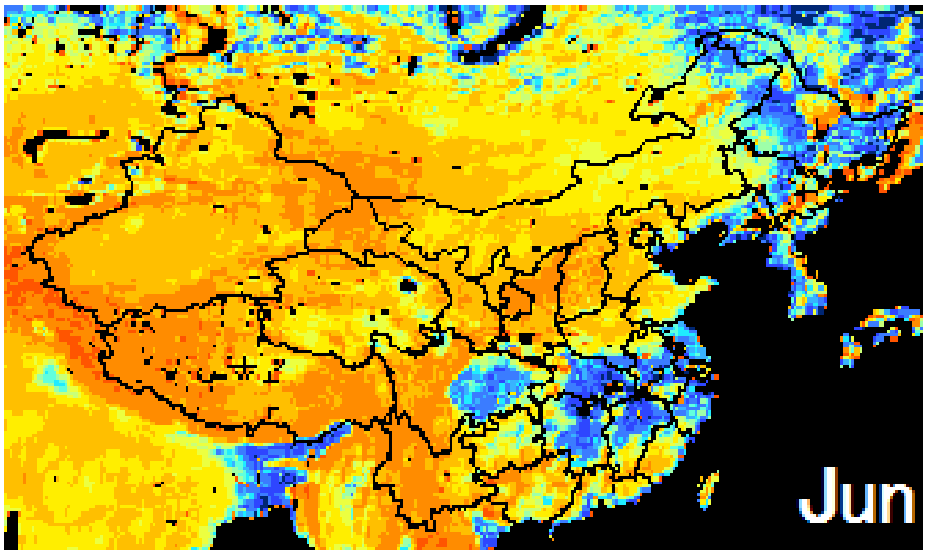

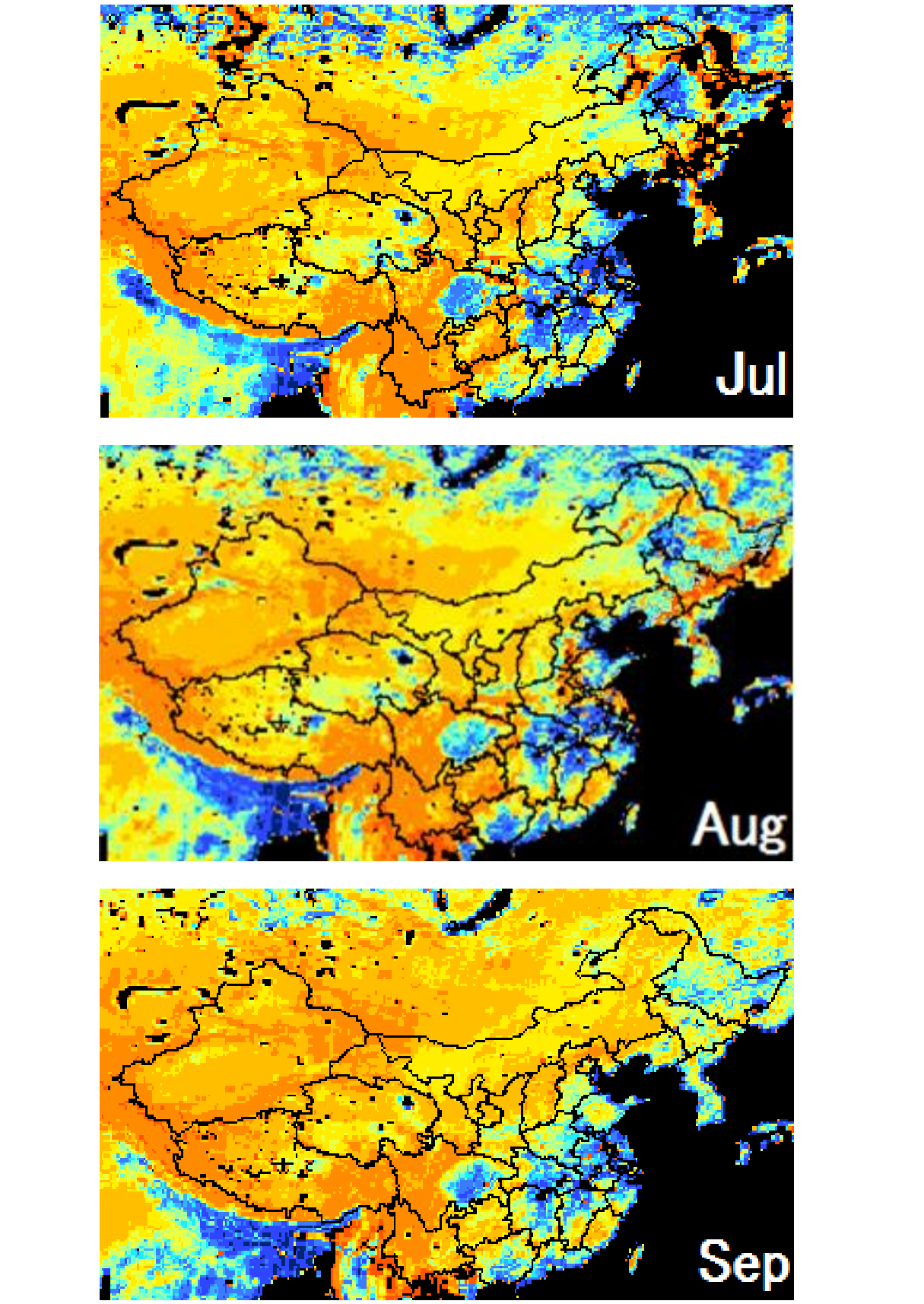

Figure 4. 12 Monthly (May to September) mean values of AMSR-E soil moisture in East Asia from 2003 to 2009.

4.4 Temporal variation of AMSR-E soil moisture and precipitation in a humid region, arid region and semi-arid region

Above, we reported a macro-scale soil moisture analysis of five sections covering a huge regions. Here we estimate the micro-scale changes in soil moisture. For this purpose, we choose three representative areas with different land types (Figure. 4.13). Figure 4.14 shows the time series of AMSR-E soil moisture and APHRODITE precipitation over different regions of China from 2002 to 2009. As the APHRODITE precipitation dataset terminated in 2007, only the AMSR-E soil moisture is available for 2008 and 2009. Overall, the soil moisture and precipitation are well matched in all four regions.

Figure 4. 13 Location and images of three representative regions in the micro-scale soil moisture analysis.

Tazhong (39° N, 83° E) occupies part of the Taklimakan Desert in northwest China. Taklimakan is the largest desert in China, and received an average annual rainfall of 30.8 mm from 2003 to 2007. Because of the low rainfall and high evaporation rate, the soil moisture was almost constant over the five years. A rainfall event in this region causes a sudden spike in the AMSR-E soil moisture.

Heshun (37.3° N, 113.6° E) is a semi-arid region located in the center of China. The average annual rainfall (2003–2007) was 569.4 mm. The moisture variation is smaller than Shunxi's and larger than Tazhong's. Over the long-term, it remains stable at approximately 0.05 m^3/m^3. In summer, it increases rapidly with rainfall, but always remains under 0.5 m^3/m^3.

Shunxi (30° N, 119° E) is located in the southeast of China, near the middle and lower Yangtze River. Being a humid region, Shunxi receives a large amount of rainfall. The average annual rainfall in 2003–2007 was 1212.4 mm, with more than 100 mm/day on some days. The soil moisture exhibited a relatively stable pattern in this area. Following a precipitation event, the soil moisture largely fluctuated even in winter, with slow increases and decreases.

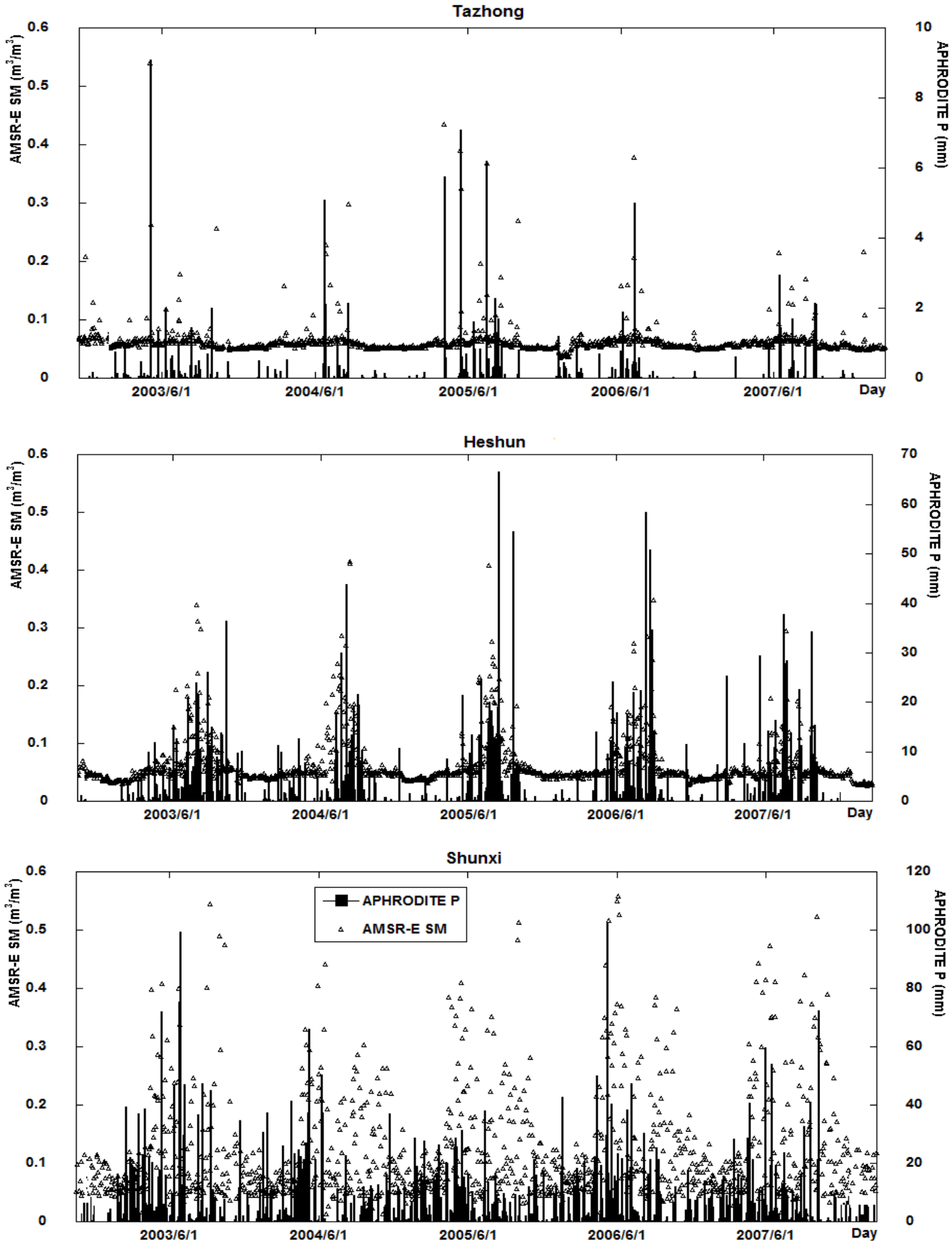

Figure 4.14 Time series of AMSR-E soil moisture and APHRODITE precipitations over different regions (Tazhong, Heshun, and Shunxi,) of China from 2003 to 2007.

In the arid and semi-arid regions (Heshun and Tazhong), the daily soil moisture rapidly increased after a rain event, then rapidly decreased as the water evaporated and was not replaced (Shinoda, 2005). On the other hand, the soil moisture in the humid region (Shunxi) was stored for a few days after the rainfall. Therefore, whereas the soil moisture spikes in relatively dry regions, it ascends and descends rather more slowly in humid regions. These characteristics, which are also seen in Figure. 4.14, highlight the need for measuring soil moisture variation on daily scales. (Koster et al., 2001) proposed that soil moisture has a "memory;" that is, the soil can "remember" wet and dry conditions. This memory causes an anomaly long after the conditions have been forgotten by the atmosphere. It is also linked to another phenomenon, namely, that soil moisture reflects the impact of the precipitation regime (Orth and Seneviratne, 2012). In summary, the soil memory is small in arid regions and large in humid regions.

4.5 Conclusions

This chapter summarized the spatial and temporal variations and distributions (also called the dynamic behaviors) of the soil moisture in East Asia. Because of the monsoon climate in East Asia, the soil moisture was high in summer and low in winter. Generally, the soil moisture was higher in the east coastal areas than in west continental regions. In a nine-year analysis, the characteristics of the AMSR-E soil moisture showed regional differences. In addition, the macro-scale changes in soil moisture were analyzed in representative areas from 2003 to 2009. The main conclusions are presented below:

In the middle and lower Yangtze River Plain, the soil moisture content remained above 0.06 m^3/m^3 even in winter, and peaked at 0.6 m^3/m^3 in summer. During the rainy season (June and July), the AMSR-E soil moisture closely followed the Baiu front on both daily and monthly timescales. Moreover, in a daily soil moisture analysis at Bengbu near Huaihe River in July 2003, the AMSR-E soil moisture captured the flood record, and remained

high for several days after a large rainfall event in humid regions.

In Sichuan Basin, the monthly mean soil moisture was directly related to the monthly mean precipitation. In the land use map, most of the areas were covered by paddy fields. The soil moisture in a paddy area peaked twice in one year; during transplanting, and again during canopy closure. Therefore, the farming calendar of paddy exerts an important influence on soil moisture in this region. A negative relationship between AMSR-E soil moisture and NDVIs was observed in September and October; the soil moisture declined during the growing season for rice. The AMSR-E soil moisture appeared to estimate the double-cropping pattern of paddy in this region, providing a route for agricultural production and evaluation.

Additionally, we analyzed the micro-scale soil moisture variations in three areas with different climates (humid region, arid region, and semi-arid region). The representative areas (Shunxi, Tazhong, and Heshun) were selected by comparing many candidate areas. The soil moisture varied much more widely in the humid area (Shunxi) than in the arid and semi-arid areas (Heshun and Tazhong, respectively). We concluded that soil moisture is retained for several days after a rainfall event in humid regions, but is rapidly lost by evaporation in arid and semi-arid regions. This feature of soil moisture was connected to the memory of the soil moisture in the area. In conclusion, daily satellite imaging of soil moisture by AMSR-E captures the spatial and temporal features and variations of soil moisture over large regions.

Chapter Ⅴ. General conclusions

This study evaluated an AMSR-E soil moisture product, namely, a satellite-based dataset of surface soil moisture, in comparisons with ground-based data collected over Shanxi Province of China. From the AMSRE-E data, we spatio-temporally characterized the distributions and variations of soil moisture over East Asia.

The major results of the evaluation are summarized below.

(1) The AMSR-E soil moisture product was evaluated at high spatial resolution (50 × 50) km^2 over Shanxi Province, China. Good evaluation results in 2006 and 2007 were obtained over most areas. The AMSR-E soil moisture product (Version.5.31) proved very effective for surface soil moisture monitoring.

(2) The AMSR-E and ground-based datasets were well correlated (correlation coefficient > 0.7) in regions with uniform land use type and relatively flat terrain. The density of the situ observation stations was also important. The correlation coefficients were low in areas with only one or two stations, and high in areas averaging 5–7 stations. Increasing the number of in situ observation stations would certainly improve the evaluations. Therefore, the number of in situ observation stations must be considered in the validation results.

(3) The soil moisture in Shanxi Province tended to increase from northwest to southeast, concordant with the APHRODITE precipitation dataset. The soil moisture well corresponded to the precipitation over Shanxi Province on all timescale (annual, monthly, and daily). Divergences between soil moisture and precipitation were attributed to different observation timings and the influence of irrigation on agricultural areas.

(4) The AMSR-E soil moisture were highly correlated with the SPOT/VEGETATION NDVI, over the whole Shanxi Province and in five representative areas. The average NDVI generally increased with soil moisture. However, AMSR-E soil moisture was difficult to evaluate in dense forest areas.

The AMSR-E soil moisture product also revealed the following dynamic behaviors of the soil moisture throughout East Asia.

(5) Soil moisture was mainly affected by rainfall in the middle and lower Yangtze River Plain. In this area, the AMSR-E soil moisture were consistent with the APHRODITE precipitation data. The AMSR-E soil moisture data captured the flood records at Bengbu near Huaihe River in 2003, and the movement of the rainy season in June and July of 2005 (identified in a weather map).

(6) In Sichuan Basin, a region famous for its rice cultivation in China, the relationship between soil moisture and precipitation was less obvious. When evaluated over a paddy area throughout 2006, the AMSR-E soil moisture exhibited two obvious peaks. Comparison with the farming calendar (rice transplanting and harvest seasons) confirmed that these soil moisture variations were linked to irrigation (human activity).

(7) In arid and semi-arid regions, the AMSR-E soil moisture sharply spiked after a rainfall event, whereas in humid regions, a rainfall event caused a slow rise and fall of the soil moisture. Specifically, the AMSR-E soil moisture remained for several days after the rainfall in humid regions, but quickly evaporated in dry regions. Furthermore, the monthly and annual analysis of variations in the surface soil moisture indirectly reflect the local memory span of the soil moisture.

Many phenomena remain to be investigated in AMSR-E soil moisture researches. Examples are the relationship between the ground conditions (surface soil moisture) and frequency of dust events in East Asia, and the effect of vegetation phenology on the soil moisture variation in Outer Mongolia. Thus, a rich body of new insights is expected to emerge from future researches on AMSR-E soil moisture.

REFERENCES

Beljaars, A.C.M., Viterbo, P., Miller, M., Betts, A.K. 1996. The anomalous rainfall over the United States during July 1993: sensitivity to land surface parameterization and soil moisture anomalies. Monthly Weather Review 124 (3): 362-382. DOI: 10.1175/1520-0493(1996)124.

Bosilovich, M.G., and Sun, W.Y. 1999. Numerical Simulation of the 1993 Midwestern flood: land-atmosphere interactions. *Journal of Climate* 12: 1490-1505. DOI: 10.1175/1520-0442(1999)012<1490:NSOTMF>2.0.CO;2.

Calvet, J.C., Fritz, N., Froissard, F., Suquia, D., Petitpa, A., Piguet, B. 2007. In situ soil moisture observations for the CAL/VAL of SMOS: the SMOSMANIA network. *Geoscience and Remote Sensing Symposium*. IGARSS: 1196–1199. DOI: 10.1109/IGARSS.2007.4423019.

Chaurasia, S., Tung, D. T., Thapliyal, P.K., Joshi, P.C. 2011. Assessment of AMSR-E soil moisture product over India. *International Journal of Remote Sensing* 32 (23): 7955-7970. DOI: 10.1080/01431161.2010.531782.

Draper, C.S., Walker, J.P., Steinle, P.J., De jeu, R.A.M., Holmes, T.R.H. 2009. An evaluation of AMSR-E derived soil moisture over Australia. *Remote Sensing of Environment* 113: 703-710. DOI: 10.1016/ j.rse.2008.11.011.

Eymard, L., Bernard, R. and Lojou, J.Y., 1993, Validation of microwave radiometer geophysical parameters using meteorological model analysis. International Journal of Remote Sensing, 14, pp. 1945–1963.

Fu, B., Wang, J., Chen, L.,Qiu, Y. 2003.The effects of land use on soil moisture variation in the Danangou catchment of the Loess Plateau, China. *Science direct Catena* 54:197-213. DOI: 10.1016/S0341-8162(03)00065-1

Jackson, T.L. 1993. Measuring surface soil moisture using passive microwave remote

sensing. *Hydrological Processes* 7 (2): 139-152. DOI: 10.1002/hyp. 3360070205.

Hillel, D. 1998. *Environmental Soil Physics*. Academic Press: San Diego; 771.

Kaihotsu, I., Koike, T., Yamanaka, T., Fujii, H., Ohta, T., Tamagawa, K., Oyunbaatar, D., Akiyama, R. 2009. Validation of soil moisture estimation by AMSR-E in the Mongolian Plateau. *Journal of the Remote Sensing Society of Japan* 29 (1): 271-281.

Koike, T., Shimo, C., Ohta, T., Fujii, H., Shibata, A. 2000. Development and validation of a microwave radiometer algorithm for land surface hydrology. *Journal of Japan Society of Civil Engineers* B 44: 247-252. DOI: 10.2208/prohe.44.247.

Koike, T., Nakamura, Y., Kaihotsu, I., Davaa, G., Matsuura, N., Tamagawa, K., Fujii, H. 2004. Development of an advanced microwave scanning radiometer (AMSR-E) algorithm for soil moisture and vegetation water content. *Journal of Japan Society of Civil Engineers* B 48: 217-222. DOI: 10.2208/prohe (in Japanese).

Koster, R.D., Suarez, M.J. 2001. Soil moisture memory in climate models. *Journal of Hydrometeorology* 2 (6): 558-570. DOI: 10.1175/1525-7541(2001)002.

Klemas, V., Finkl, C.W., Kabbara, N. 2014. Remote sensing of soil moisture: An overview in relation to coastal soils. *Journal of Coastal Research* 30(4): 685-696. DOI: 10.2112/JCOASTRES-D-13-00072.

Konda, M., Ichikawa, H., Tomita, H. 2009. Wind speed and latent heat flux retrieved by simultaneous observation of multiple geophysical parameters by AMSR-E. *Journal of the Remote sensing society of Japan* 29(1): 191-198. DOI: 10.1175/JAMC-D-11-0209.1.

Lu, H., Koike, T., Fujii, H., Ohta, T., Tamagawa, K. 2009. Development of a physically-based soil moisture retrieval algorithm for spaceborne passive microwave radiometers and its application to AMSR-E. Journal of The Remote Sensing Society of Japan 29 (1): 253-262. DOI:10.11440/rssj.29.253

Moran, M.S. 1994. Irrigation management in Arizona using satellites and airplanes. *Irrigation Science* 15(1): 35-44. DOI: 10.1007/BF00187793.

Michiura, T. 2011. Current situation and achievements of advanced microwave scanning radiometer for-Earth Observing System (AMSR-E). *Japan Aerospace Exploration Agency (JAXA)* http://www.jaxa.jp/press/2011/10/20111012_sac_AMSR-E_j.html (in Japanese).

Michiura, T. 2011. "Current status and outcomes of AMSR-E" Japan Aerospace eXploration Agency. http://www.jaxa.jp/press/2011/10/20111012_sac_AMSR-E_j.html. (reference: 2014/10/20)

Niu, J.X., Zhao, J.B. 2008. Soil moisture environment and vegetation construction in Shanxi Province. *China Environmental Science Press*10-29 (in Chinese).

Njoku, E.G., Jackson, T.L., Lakshmi, V., Chan, T., Nghiem, S.V. 2003. Soil moisture retrieval from AMSR-E. *IEEE Transactions on Geoscience and Remote Sensing* 41(2): 215-229. DOI: 10.1109/TGRS.2002.808243.

NASA (National Aeronautics and Space Administration). 2008. "Atmospheric electromagnetic transmittance or opacity".https://commons.wikimedia.org/wiki/File: Atmospheric _electromagnetic_transmittance_or_opacity.jpg (reference: 2016/7/10).

Owe, M., De jeu R.A.M., Walker, J. 2001. A methodology for surface soil moisture and vegetation optical depth retrieval using the microwave polarization difference index. *IEEE Transactions on Geoscience and Remote Sensing* 39 (8): 1643-1654. DOI: 10.1109/36.942542.

Orth, R., Seneviratne, S.I. 2012. Analysis of soil moisture memory from observations in Europe. Journal of Geophysical research 117.D15115. DOI: 10.1029/2011JD017366.

Pal, J.S., and Eltahir, E. A.B. 2001. Pathways relating soil moisture conditions to future summer rainfall within a model of the land-atmosphere system. *Journal of Climate* 15: 1227-1242. DOI: 10.1175/1520-0442(2001)014<1227:PRSMCT>2.0.CO;2.

Rossato, L., De jeu, R.A.M., Alvalá, R.C.D.S., Souza, S. 2013. Evaluation of soil moisture from satellite observations over South America. *International Journal of Remote*

Sensing 32(23): 8013-8031. DOI: 10.1080/01431161.2010.532169.

Ren, M.O., Abe, Z., Komai, S. 1986. Natural geography of China. *Tokyo University Press* (in Japanese).

Rüdiger, C., Hancock G., Hemakumara, H.M., Jacobs, B., Kalma, J.D., Martinez, C., Thyer, M., Walker, J.P., Wells, T., Willgoose, G.R. 2007. The Goulburn River experimental catchment data set. *Water Resources Research* 43: W10403. DOI: 10.1029/2006WR005837.

Sabater, J.M., Jarlan, L., Calvet, J., Bouyssel, F., De Rosnay, P. 2007. From near-surface to root-zone soil moisture using different assimilation techniques. *Journal of Hydrometeorology* 8: 194–206. DOI: 10.1175/JHM571.1.

Seth, A., and Giorgi, F. 1998. The effects of domain choice on summer precipitation simulation and sensitivity in a regional climate model. *Journal of Climate* 11: 2698-2712. DOI: 10.1175/1520-0442(1998)011<2698:TEODCO>2.0.CO;2.

Solomon, S., Qin, D.H., Manning, M., Chen, Z., Marquis, M., Averyt, K.B., Tignor, M., Miller, H.L. (Eds.) 2007. IPCC Climate Change 2007: The Physical Science Basis. Contribution of Working Group I to the Fourth Assessment Report of the Intergovernmental Panel on Climate Change. *Cambridge University Press* 996.

Shinoda, M. 2005. Soil moisture memory in arid regions: its fuction and significance of research. *Journal of Arid Land Studies* 14 (4): 185-197. DOI: 10.2208/prohe.44.247 (in Japanese).

Sun, Y.Y., Sun, Y.J., Qin, J., Yang, Z.Y., Chen, L., Xu, H., Ma, J. 2013. Temporal and spatial variation of safe sowing data in different rice cultivation zones in Sichuan. *Chinese Journal of Agrometeorology* 34(1): 58-63. DOI: 10.3969/j.issn.1000-6362.2013.01.009 (in Chinese).

Wigneron, J.P., Calvet, J.C., Pellarin, T., Van de Griend, A.A., Berger, M., Ferrazzoli, P. 2003. Retrieving near-surface soil moisture from microwave radiometric observation:

current status and future plans. *Remote Sensing of Environment* 85: 489-506. DOI: 10.1016/S0034-4257(03)00051-8.

Wang, L., John, J.Q.U. 2009. Satellite remote sensing applications for surface soil moisture monitoring: A review. *Front. Earth Sci. hina* 3(2): 237-247. DOI: 10.1007/s11707-009-0023-7.

Yatagai, A., Arakawa, O., Kamiguchi, K., Kawamoto, H., Nodzu, M., Hamada, A. 2009. A 44-year daily gridded precipitation dataset for Asia based on a dense network of rain gauges. *SOLA* 5: 137-140. DOI: 10.2151/sola, 2009-035.

Yatagai, A., Kamiguchi, K., Arakawa, O., Hamada, A., Yasutomi, N., Kitoh, A. 2012. APHRODITE: Constructing a long-term daily gridded precipitation dataset for Asia based on a dense network of rain gauges. *Bulletin of the American Meteorological Society* 93 (9): 1401-1415. DOI: 10.1175/ BAMS-D-11-0 0122.1.